



HAL
open science

Evolution of the North Anatolian Fault from a diffuse to a localized shear zone in the North Aegean Sea during the Plio-Pleistocene

M Rodriguez, D Sakellariou, Christian Gorini, A Janin, Elia d'Acremont, Laetitia Le Pourhiet, Nicolas Chamot-Rooke, K Tsampouraki-Kraounaki, I Morfis, G Rousakis, et al.

► To cite this version:

M Rodriguez, D Sakellariou, Christian Gorini, A Janin, Elia d'Acremont, et al.. Evolution of the North Anatolian Fault from a diffuse to a localized shear zone in the North Aegean Sea during the Plio-Pleistocene. *Geophysical Journal International*, 2023, 235 (3), pp.2614-2639. 10.1093/gji/ggad364 . hal-04309118

HAL Id: hal-04309118

<https://hal.science/hal-04309118v1>

Submitted on 27 Nov 2023

HAL is a multi-disciplinary open access archive for the deposit and dissemination of scientific research documents, whether they are published or not. The documents may come from teaching and research institutions in France or abroad, or from public or private research centers.

L'archive ouverte pluridisciplinaire **HAL**, est destinée au dépôt et à la diffusion de documents scientifiques de niveau recherche, publiés ou non, émanant des établissements d'enseignement et de recherche français ou étrangers, des laboratoires publics ou privés.



Evolution of the North Anatolian Fault from a diffuse to a localized shear zone in the North Aegean Sea during the Plio-Pleistocene

Journal:	<i>Geophysical Journal International</i>
Manuscript ID	GJI-23-0096.R1
Manuscript Type:	Research Paper
Date Submitted by the Author:	n/a
Complete List of Authors:	Rodriguez, Mathieu; Ecole Normale Supérieure, geosciences Sakellariou, Dimitris; Hellenic Center for Marine Research, Institute of Oceanography Gorini, Christian; Institut des Sciences de la Terre de Paris Janin, Alexandre; Laboratoire de Géologie de l'Ecole Normale Supérieure d'Acremont, Elia; Université Pierre et Marie Curie, ISTEP le pourhiet, laetitia; Sorbonne University Chamot-Rooke, Nicolas; CNRS Ecole normale supérieure, Laboratoire de Géologie Tsampouraki-Kraounaki, Konstantina; Hellenic Center for Marine Research Morfis, Iannis; Hellenic Center for Marine Research Rousakis, George; Hellenic Center for Marine Research Henry, Pierre; CEREGE Lurin, Aude; Université Toulouse III Paul Sabatier Delescluse, Matthias; Laboratoire de Géologie de l'Ecole Normale Supérieure Briole, Pierre; Laboratoire de Géologie de l'Ecole Normale Supérieure, Laboratoire de Géologie Rigo, Alexis; Laboratoire de Géologie de l'Ecole Normale Supérieure Arsenikos, Stavros; Beicip-Franlab Bulois, Cédric; Laboratoire de Géologie de l'Ecole Normale Supérieure Fernandez Blanco, david; Instituto de Ciencias del Mar Beniest, Anouk; Vrije Universiteit Amsterdam Grall, Celine; La Rochelle Université Chanier, Frank; Université de Lille Faculté des Sciences et Technologies Caroir, Fabien; Université de Lille Faculté des Sciences et Technologies Dessa, Jean-Xavier; UPMC, Géoazur Oregioni, Davide; GeoAzur Necessian, Alexandre; Institut de Physique du Globe de Paris, UMR CNRS 7154
Additional Keywords:	
Keywords:	Transform faults < TECTONOPHYSICS, Submarine tectonics and volcanism < TECTONOPHYSICS, Continental tectonics: strike-slip and transform < TECTONOPHYSICS

1
2
3
4
5
6
7
8
9
10
11
12
13
14
15
16
17
18
19
20
21
22
23
24
25
26
27
28
29
30
31
32
33
34
35
36
37
38
39
40
41
42
43
44
45
46
47
48
49
50
51
52
53
54
55
56
57
58
59
60



1 **Evolution of the North Anatolian Fault from a diffuse to a localized shear zone in the North**

2 **Aegean Sea during the Plio-Pleistocene**

3 Rodriguez, M. ¹; Sakellariou, D. ²; Gorini, C. ³; Janin, A. ¹; D'Acemont, E. ³; LePourhiet, L. ³; Chamot-
 4 Rooke, N. ¹; Tsampouraki-Kraounaki, K. ²; Morfis, I. ²; Rousakis, G. ²; Henry, P. ⁴; Lurin, A. ¹;
 5 Delescluse, M. ¹; Briole, P. ¹; Rigo, A. ¹; Arsenikos, S. ⁵; Bulois, C. ¹; Fernández-Blanco, D. ⁷; Beniést,
 6 A. ⁸; Grall, C. ⁹; Chanier, F. ¹⁰; Caroir, F. ¹⁰; Dessa, J-X. ⁶; Oregioni, D. ⁶; Nercessian, A. ¹¹

7
 8 *1 - Laboratoire de Géologie, Ecole normale supérieure, PSL research university, CNRS UMR 8538, 24*
 9 *rue Lhomond, 75005 Paris, France*

10 *2- Institute of Oceanography, Hellenic Center of Marine Research, GR-19013 Anavysos, Greece*

11 *3-Sorbonne Université, UPMC Université Paris 06, UMR 7193, IStEP, F-75005, Paris, France.*

12 *4- Centre Européen de Recherche Et d'Enseignement Des Géosciences de L'Environnement, Aix-*
 13 *Marseille Université, Marseille, France*

14 *5- Beicip-Franlab, Rueil-Malmaison, France*

15 *6- Géoazur, Université de Nice-Sophia Antipolis-CNRS-OCA, France*

16 *7- Barcelona Center for Subsurface Imaging, Instituto de Ciencias del Mar, CSIC, Barcelona, Spain*

17 *8- Department of Earth Sciences, Vrije Universiteit Amsterdam, Amsterdam, the Netherlands*

18 *9- LIENSs, La Rochelle University, La Rochelle, France*

19 *10- Univ. Lille, CNRS, Univ. Littoral Côte d'Opale, UMR 8187, LOG, Laboratoire d'Océanologie et de*
 20 *Géosciences, F59000 Lille, France*

21 *11- Université de Paris, Institut de physique du globe de Paris, CNRS, F-75005 Paris, France*

22 **Abstract**

23 **The North Anatolian Fault is the ~1200-km-long active continental transform boundary between**
 24 **Anatolia and Eurasia. This strike-slip system initiated around 10-12 Ma and experienced**
 25 **diachronous episodes of strain localization along its strike. The structural evolution of the ~350-**
 26 **km-long fault segments crossing the North Aegean Sea remains to be accurately investigated.**
 27 **There, the modern North Anatolian Fault is localized along two main branches: the northern**
 28 **branch ends at the North Aegean Trough and the southern branch ends at the Edremit-Skyros**

1
2
3 29 **Trough. The Evia Basin is located in the North Aegean Domain between the North Anatolian Fault**
4
5 30 **and the Corinth Rift. This study presents seismic reflection lines crossing the aforementioned**
6
7 31 **structures of the North Aegean Domain, which document their subsurface structure and the**
8
9 32 **sedimentary record of their activity since the Messinian. The seismic-reflection dataset is tied to**
10
11 33 **regional-scale stratigraphic markers, which constrains the age of main tectonic events related to**
12
13 34 **the formation of the North Anatolian Fault. The seismic-reflection lines show that the two main**
14
15 35 **branches of the North Anatolian Fault became localized structures at 1.3-2 Ma, coevally with the**
16
17 36 **formation of the Evia Basin. Since 2 Ma, the North Aegean Troughs developed as a series of**
18
19 37 **horsetail basins propagating westwards at the termination of the branches of the North Anatolian**
20
21 38 **Fault. On a regional scale, the wide and diffuse North Anatolian transtensive shear zone active**
22
23 39 **from Serravalian to Late Pliocene turned into a narrower shear zone at the two main branches of**
24
25 40 **the North Anatolian Fault since the Early Pleistocene. This abrupt episode of strain localization**
26
27 41 **occurred in the frame of the major Early Pleistocene change in stress regime from NE-SW to N-**
28
29 42 **S extension, which has been observed throughout the Aegean Sea.**
30
31
32
33
34

35 44 **Keywords:** *Continental tectonics; strike-slip and transform; Transform faults; Normal faulting;*
36
37 45 *Tectonics and landscape evolution; Europe; Crustal imaging.*
38
39 46

41 47 **1- Introduction**

42
43 48 Transform faults are major lithospheric-scale tectonic structures acting as plate boundaries (Woodcock,
44
45 49 1986; Mann, 2007), along which relative plate motion occurs horizontally along the fault's strike. The
46
47 50 accumulated relative plate motion along transform boundaries juxtaposes sections of the lithosphere
48
49 51 with different histories, ages, and hence, mechanical properties (Ben Zion & Sammis, 2003). The
50
51 52 complex rheology of the continental domain results in both localized (e.g. the Dead Sea Fault; Garfunkel
52
53 53 & Ben-Avraham, 1996) and diffuse continental transform systems (e.g. the Trans-Alboran Shear Zone;
54
55 54 Lafosse *et al.*, 2020). Some transform systems have also being shown to alternate localized and diffuse
56
57 55 strain along their strike (e.g. the San Andreas Fault; Wesnousky, 2005; and the North Anatolian Fault;
58
59 56 Sengör *et al.*, 2019).

1
2
3 57 Field studies reveal that continental transforms initiate as several hundreds of kilometers-wide
4
5 58 distributed areas of deformation, forming a shear zone that is composed of scattered oblique en-échelon
6
7 59 strands (Tchalenko & Ambraseys, 1970; Sengör *et al.*, 2005; Wesnousky, 2005; Mann, 2007; Sengör *et*
8
9 60 *al.*, 2014). During fault initiation, motion is distributed over several individual fault segments. As finite
10
11 61 relative motion increases, fault strands progressively connect into continuous and localized strike-slip
12
13 62 fault segments. The increased connection of fault strands shapes narrower shear zones (<100-km- wide)
14
15 63 with local structural complexities in stepover (releasing or restraining bends). The localization of strike-
16
17 64 slip segments leaves some initial oblique strands deactivated. The timing of strain localization within
18
19 65 the wide shear zone may differ from one fault segment to another. The lifetime of such shear systems in
20
21 66 the continental setting is in the order of 10^7 yrs (Sengör *et al.*, 2019). Analog models reproduce the
22
23 67 transition from an initial diffuse shear zone composed of Riedel faults to a localized fault formed by the
24
25 68 linkage of shear segments (Tchalenko, 1970; Dooley & Schreurs, 2012; Lefevre *et al.*, 2020).

26
27
28 69 The North Anatolian Fault system, located in the Eastern Mediterranean domain (Fig. 1, 2), is the 1200-
29
30 70 km-long dextral strike-slip boundary between the Anatolian and Eurasian tectonic plates (Fig. 1, 2),
31
32 71 which connects the Anatolia-Arabia-Eurasia triple junction in the East (Hubert Ferrari *et al.*, 2010) to
33
34 72 the Hellenic Subduction Zone (Flerit *et al.*, 2004; Sakellariou *et al.*, 2018; Ferentinos *et al.*, 2018). The
35
36 73 North Anatolian Fault triggers frequent earthquakes above $M_w \sim 7$ (e.g. Izmit and Duzce events in 1999;
37
38 74 Hubert-Ferrari *et al.*, 2000; Bulut *et al.*, 2018) and its submarine segments are a potential source of
39
40 75 tsunamis (Hébert *et al.*, 2005; Reicherter *et al.*, 2010; Janin *et al.*, 2019).

41
42
43 76 The North Anatolian Fault transects continental lithosphere with significant along-strike strength
44
45 77 variations, inherited from the successive geological events that shaped the Hellenides mountain belt
46
47 78 prior to its collapse. As such, the North Anatolian Fault is a relevant case-study of a post-orogenic
48
49 79 transform fault (Le Pourhiet *et al.*, 2014; Jolivet *et al.*, 2021).

50
51 80 The objective of this study is to constrain the structural evolution of the ~350-km-long segment of the
52
53 81 North Anatolian Fault crossing the North Aegean Sea (Fig. 3, 4), on the basis of a set of multibeam data
54
55 82 (Ypother cruises, 2013-2016; Sakellariou *et al.*, 2018) and seismic-reflection profiles (NAFAS cruise,
56
57 83 2017; Rodriguez *et al.*, 2018; vintage seismic lines published in Beniest *et al.*, 2016).

1
2
3 84 The present dataset covers some of the major tectonic structures encountered in the North Aegean
4
5 85 Domain, namely the North Aegean Trough, the Edremit-Skyros Trough and the Evia Basin (Fig. 2-4).
6
7 86 There, the different steps of formation of the North Anatolian Fault remained poorly constrained due to
8
9 87 the lack of seismic-reflection and stratigraphic data (Krijgsman *et al.*, 2022). We define some regional
10
11 88 stratigraphic markers for the period spanning the Messinian to the present-day (Laigle *et al.*, 2000;
12
13 89 Beniest *et al.*, 2016; Ferentinos *et al.*, 2018) to reach a precision in the ages of tectonic events
14
15 90 comparable to the segments of the North Anatolian Fault observed in the Marmara Sea (Le Pichon *et*
16
17 91 *al.*, 2014). Finally, we provide structural maps of the post-Messinian evolution of the North Aegean
18
19 92 Domain, from the Yeniçağa Fork east of Marmara to the Evia Basin in Greece (Fig. 2). Overall, our
20
21 93 structural reconstructions of the North Anatolian Fault document the strain localization within a post-
22
23 94 orogenic continental shear zone and the time of effective formation of such tectonic plates.
24
25
26
27
28

29 96 **2- Geological Background**

30 97 **2-1-Present-day configuration of the North Anatolian Fault in the North Aegean Domain**

31
32 98 The North Anatolian Fault is the plate boundary between Anatolia and Eurasia, with a current dextral
33
34 99 strike-slip rate of 23 mm.yr⁻¹ (Le Pichon *et al.*, 2003; Reilinger *et al.*, 2006; Le Pichon & Kreemer, 2010;
35
36 100 Pérouse *et al.*, 2012; Müller *et al.*, 2013). The finite amount of dextral motion along the North Anatolian
37
38 101 Fault is estimated to 85±5 km, with some ambiguities in areas where slip is distributed over several fault
39
40 102 strands (Sengör *et al.*, 2005). The finite offset results from strike-slip rates that grew from ~3 mm.yr⁻¹
41
42 103 in the earliest stages of formation of the fault system to near-current slip rates since the Early Pleistocene
43
44 104 (Hubert Ferrari *et al.*, 2010).

45
46 105 In this study, the North Aegean Domain is defined as the area bounded to the south by the North Cycladic
47
48 106 Detachment System, to the north by the Rhodope Detachment System, to the west by the Vardar Suture
49
50 107 Zone and to the East by the Yeniçağa fork (Fig. 1, 2). The total amount of slip-rate along the North
51
52 108 Anatolian Fault is accommodated by its northern and southern branches in the North Aegean Domain
53
54 109 (Fig. 1, 2; Le Pichon *et al.*, 2003).

55
56 110 The northern branch of the North Anatolian Fault crosses the Marmara Sea (i.e. the Main Marmara
57
58 111 Fault; Le Pichon *et al.*, 2001), then runs along the Gelibolu Peninsula and the Gulf of Saros until it

1
2
3 112 connects the North Aegean Trough (Fig. 2). The North Anatolian Fault makes a $\sim 30^\circ$ bend at the
4
5 113 connection between the Saros Gulf and the North Aegean Trough (Roussos & Lyssimachou, 1991;
6
7 114 Koukouvelas & Aydin, 2002). The strike-slip rate of relative motion along the northern branch decreases
8
9 115 from 21.2 mm yr^{-1} at the Gulf of Saros to $\sim 5 \text{ mm yr}^{-1}$ at the Sporadhes archipelago (Müller *et al.*, 2013).
10
11 116 The southern branch of the North Anatolian Fault crosses the Biga Peninsula and connects the Edremit-
12
13 117 Skyros Trough in the Aegean Sea (Fig. 2). The strain distribution of the southern branch of the North
14
15 118 Anatolian Fault (Fig. 2-4) is diffuse onland in Turkey (Sümer *et al.*, 2018), whereas it is expressed as a
16
17 119 localized structure offshore (Papanikolaou *et al.*, 2019). The strike-slip rate along the southern branch
18
19 120 is on the order of 10 mm.yr^{-1} (Müller *et al.*, 2013).
20
21
22 121 Both the North Aegean and the Edremit-Skyros Troughs reveal horsetail structures (Fig. 3-4). Horsetail
23
24 122 structures are commonly observed at the termination of strike-slip faults (Basile & Brun, 1999): they
25
26 123 consist in numerous oblique splays rooting on the main strike-slip faults and isolating a series of
27
28 124 transtensive basins. On one hand, the North Aegean Trough is $\sim 150\text{-km}$ -long, up to 80-km -wide and
29
30 125 1600-m -deep (Brooks & Ferentinos, 1980; Papanikolaou *et al.*, 2002; Sakellariou *et al.*, 2018;
31
32 126 Ferentinos *et al.*, 2018), running from the Lemnos Deep to the Sporadhes archipelago (Fig. 3, 4). On the
33
34 127 other hand, the Edremit-Skyros Trough is 70-km -long, up to 50-km -wide, and 1050-m -deep (Fig. 3, 4;
35
36 128 Papanikolaou *et al.*, 2019). There, the southern branch of the North Anatolian Fault acts as a marginal
37
38 129 structure, which bounds the southern flank of the trough over its entire length and splits into two 45 to
39
40 130 66-km -long oblique splays isolating sub-basins.
41
42
43 131

45 132 **2-2- Tectonic configuration of the North Anatolian Fault in the North Aegean Domain since the** 46 47 133 **Middle Miocene**

48
49 134 The formation of the North Anatolian Fault results from the influence of several geodynamic drivers,
50
51 135 including Arabia-Eurasia collision, the dynamics of the Hellenic trench retreat and the resulting
52
53 136 differential in gravitational potential between the Anatolian plateau and the Aegean Sea (Jolivet &
54
55 137 Faccenna, 2000; Faccenna *et al.*, 2006; Brun & Faccenna, 2008; Le Pourhiet *et al.*, 2012; Jolivet *et al.*,
56
57 138 2015; Brun *et al.*, 2016; England *et al.*, 2016).
58
59
60

1
2
3 139 Most of the constraints on the history of the North Anatolian Fault in the North Aegean Domain are
4
5 140 based on the study of the Marmara Sea and its surroundings. At least three successive major strike-slip
6
7 141 systems, evolving into a continuous frame of shearing of the continental lithosphere, have been
8
9 142 identified on the basis of seismic data tied to industrial wells (Sengör *et al.*, 2014; Le Pichon *et al.*, 2014;
10
11 143 2015).

13 144 A first diffuse strike-slip system emplaced in Late Serravalian-Tortonian (12-10 Ma), in the area that is
14
15 145 now enclosed between the Thrace basin and the Sakarya suture (Fig. 1, 2). A part of this first strike-slip
16
17 146 system is still active as the southern branch of the North Anatolian Fault, where the pattern of drainage
18
19 147 networks recorded a structural reorganization around 0.5-1.3 Ma (Demoulin *et al.*, 2013).

21 148 A second strike-slip system is evidenced at the South Marmara Fault and the Ganos segment, both
22
23 149 corresponding to positive flower structures formed at a restraining bend (Fig. 2; Le Pichon *et al.*, 2014;
24
25 150 2015; Karakas *et al.*, 2018). These structures record the beginning of the localization of the North
26
27 151 Anatolian Shear System in the Pliocene (Armijo *et al.*, 1999; Le Pichon *et al.*, 2014; 2015). The South
28
29 152 Marmara Fault goes extinct around 3.5 Ma, while the Ganos segment is still active and forms a well-
30
31 153 localized, >130-km-long dextral strike-slip fault (Armijo *et al.*, 1999).

34 154 The third, localized strike-slip system corresponds to the northern branch of the North Anatolian Fault,
35
36 155 expressed as the Main Marmara Fault in the Marmara Sea (Le Pichon *et al.*, 2001; 2003; Carton *et al.*,
37
38 156 2007). Estimates of the age of the Main Marmara Fault range between 0.5 and 2.5 Ma (Rangin *et al.*,
39
40 157 2004; Grall *et al.*, 2012, 2013; Le Pichon *et al.*, 2015). The Main Marmara Fault crosses the Gelibolu
41
42 158 Peninsula and connects the Gulf of Saros at the entrance of the Aegean Sea through the Ganos strike-
43
44 159 slip segment (Fig. 2; McNeill *et al.*, 2004).

47 160 The age of formation of the North Aegean Trough and the Skyros-Edremit Trough is roughly
48
49 161 constrained in the Late Pliocene-Early Pleistocene (Laigle *et al.*, 2000; Beniest *et al.*, 2016), a period
50
51 162 which encompasses several stages of evolution of the North Anatolian Fault.

53 163 Onland, a series of sedimentary basins (Fig. 2; namely the Strymon, Orfanos, Prinos, Drama, Sandanski,
54
55 164 Mygdonia basins and grabens) formed in the Serravalian segmenting the Rhodope Metamorphic Core
56
57 165 Complex until the Early Pliocene (Brun & Sokoutis, 2018). Traces of Late Miocene extension and
58
59
60

1
2
3 166 differential subsidence are further observed in the Gulf of Thermaïkos and offshore the Chalkidiki
4
5 167 peninsula (Varesis & Anastasakis, 2021).

6
7 168

9 169 **2-3- Structure of the lithosphere in the North Aegean Domain**

11 170 In the North Aegean Domain, the continental lithosphere keeps the record of a complex geological
12
13 171 history, from the closure of Mesozoic Oceans (i.e. the Vardar and Pindos Oceans, Schettino & Turco,
14
15 172 2011; Okay & Tüysuz, 1999) to the building of the Hellenides Mountain Belt and its subsequent collapse
16
17 173 in the wake of the Early Cenozoic collision between Adria and Pelagonia domains (Handy *et al.*, 2010).

18 174 A series of metamorphic core complexes emplaced in the North Aegean Domain from the Late Eocene
19
20 175 to the Middle Miocene (Rhodope Core complex, 45-Myrs-old; North Cycladic Detachment System, 15-
21
22 176 20 Myrs-old; Jolivet & Brun, 2010; Le Pourhiet *et al.*, 2012; Jolivet *et al.*, 2013).

23
24 177 As a result, the North Aegean lithosphere displays an unusual layering, with a shallow brittle ductile
25
26 178 transition (<10 km, Brun & Sokoutis, 2018) and a thinned lithospheric mantle. The Moho depth ranges
27
28 179 between 20 and 30 km (Sodoudi *et al.*, 2006). Rayleigh wave anisotropy reveals the existence of a
29
30 180 thermal anomaly located right in between the two segments of the North Anatolian Fault in the North
31
32 181 Aegean domain, within the lower crust and the lithospheric mantle (Endrun *et al.*, 2011).

33
34
35 182

36 37 38 183 **3- Material and Methods**

39 184 **3-1- Topography & seafloor bathymetry**

40
41 185 The Digital Elevation Model used for the maps of the North Aegean Domain (Fig. 1-4) combines data
42
43 186 from the Shuttle Radar Topography Mission (SRTM) at 3 seconds and the multibeam dataset acquired
44
45 187 during the Ypother oceanographic cruises between 2013-2016 (Sakellariou *et al.*, 2018), here gridded
46
47 188 at 25 m.

48
49
50 189

51 190 **3-2- Seismic profiles**

52
53 191 In this study, we present a new seismic-reflection dataset collected during the NAFAS (North Anatolian
54
55 192 Fault in the North Aegean Sea) expedition in summer 2017, onboard the R/V Tethys II. The expedition
56
57 193 focused on the North Aegean Trough, the Edremit-Skyros Trough and the Evia Basin. The NAFAS

1
2
3 194 dataset is complementary documented by a set of vintage seismic-reflection dataset collected in the 70's
4
5 195 and partly explored in Beniest *et al.* (2016). All the seismic-reflection profiles are displayed on the
6
7 196 figures with a vertical exaggeration of 14, with their related simplified cross-section at 1:1 scale.
8
9 197 Seismic reflection profiles were shot using a GI airgun and a 24-trace streamer with 400-m maximum
10
11 198 offset. The GI gun was triggered in harmonic mode (2 x 24 cubic inches) every 6s, with an acquisition
12
13 199 speed of 4.1 knots, leading to a shot interval of 12.5 m. The trace record length is 5500 ms with a 1-ms
14
15 200 sample interval. Only 8 out of 24 traces were working with a maximum offset of 200-m and a maximum
16
17 201 CDP (Common Depth Point) fold of 4. The depth of penetration of the signal reaches about 3 seconds
18
19 202 two-way travel time (TWT). The processing workflow consists in geometry setting, water-velocity
20
21 203 normal move-out, stacking, deconvolution and Kirchhoff finite difference post-stack migration.
22
23
24
25

26 205 **3-3-Multibeam and interpretation of geological structures on seismic-reflection profiles**

27
28 206 The geological mapping of tectonic structures is based on the seafloor signature of the structure on the
29
30 207 multibeam data and the expression of these features on the seismic-reflection lines (Fig. 5). The offshore
31
32 208 structural maps provided in this study (Fig. 4-5) are slightly modified from Papanikolaou *et al.* (2002;
33
34 209 2019) and Sakellariou *et al.* (2018), considering our new seismic dataset.

35
36 210 The North Aegean Domain is dominated by a large variety of strike-slip structures (Fig. 5):

37
38 211 *-Negative flower structures:* Most of the sub-basins isolated by the oblique splays within the horsetail
39
40 212 terminations correspond to negative flower structures. The negative flower structures are bounded by
41
42 213 normal faults of opposite dip and connect into a single strike-slip fault at depth.

43
44 214 *-Transpressive structures:* They correspond to positive flower structures and push-up structures, formed
45
46 215 by a set of strike-slip faults with a reverse component.

47
48 216 Tectonic processes control the distribution of clastic sedimentary deposits in the study area (Fig. 6).
49
50 217 Prior to the onset of the North Anatolian Fault, scattered distal deltaic rivers flood the area, marked by
51
52 218 moderate incision along the thalweg. Since the onset of tectonic subsidence, the rivers form channel-
53
54 219 levee systems close to the slope break and evolve downslope into canyons with V-shape morphologies
55
56 220 (Fig. 6a). The complex distribution of faults and basins within the North Aegean Trough results in a
57
58 221 scattered distribution of submarine landslides, identified according to their multibeam signature (arcuate
59
60

1
2
3 222 scar and block falls at the edge of the slope, fig. 6c) and their related mass transport deposits (marked a
4
5 223 chaotic-to-transparent seismic facies). Some of the steepest slopes display undulated seafloor (fig. 6b),
6
7 224 underlain by a series of wavy reflectors, which could be interpreted as sediment waves resulting from
8
9 225 creeping of sediments in interaction with bottom-current controlled deposition (Faugères *et al.*, 2002;
10
11 226 Shillington *et al.*, 2012). The tectonic structures also influence the circulation of oceanic bottom-
12
13 227 currents. Where the current intensity is strong, the axis of the current is associated with a rough seafloor,
14
15 228 which is an indicator of the strong sediment sorting. The attenuation of the intensity of the oceanic
16
17 229 currents promotes the building of a series of fault-controlled contourite drifts (*sensu* Rebesco *et al.*,
18
19 230 2014). The architecture of these contourite drifts display typical sigmoid to mounded configurations
20
21 231 (Fig. 6e), characterized by important lateral thickness variations of the sedimentary layers, with pinched-
22
23 232 out reflectors close to the current axis and thicker deposits away from it. Fluid escape features are
24
25 233 commonly observed close to the main faults and on the extrados of the main rollover structures (Fig. 4).
26
27 234 Fluid escape features are expressed as dense networks of conduits leading to small offsets of the
28
29 235 sedimentary layers or undulated to chaotic series of reflectors on the seismic dataset (Fig. 6d). At the
30
31 236 seafloor, the area of fluid escape form fields of coalescing circular depressions (Fig. 5e, Papatheodorou
32
33 237 *et al.*, 1993).
34
35
36 238 The clastic input to the North Aegean Sea implies that most of the structures related to the North
37
38 239 Anatolian Fault are growth structures. The timing of formation of the strike-slip structures is constrained
39
40 240 from the age of onset of the fanning of the sediments. Although many second-order unconformities
41
42 241 linked to periodic sea-level and climatic variations are encountered in the study area (Lykousis, 2009;
43
44 242 Piper & Anastasakis, 2013), we here focus on the major unconformities corresponding to the main
45
46 243 tectonic episodes related to the evolution of the North Anatolian Shear Zone, i.e. the unconformities
47
48 244 corresponding to a significant tilt of the seafloor.
49
50
51
52

245

246 **4- Stratigraphy of the North Aegean Domain**

247 **4.1. The pre-Messinian period and the Messinian Event**

248 Field studies in the Thermaïkos, Thrace and Saros Basins document two Eocene to Oligocene silici-
249 clastic units ontop of the metamorphic basement (Turgut & Eseller, 2000; Siyako & Huvaz, 2007;

1
2
3 250 Islamoglu *et al.*, 2008). Seismic profiles tied to wells evidence the continuity of these units offshore in
4
5 251 the North Aegean Domain, with a major angular unconformity at the Oligocene-Miocene boundary
6
7 252 (Beniest *et al.*, 2016; Varesis & Anastasakis, 2021). Industrial wells located in the Prinos Basin
8
9 253 (Proedrou & Papaconstantinou, 2004) provide precise constraints on the ages of the geological events
10
11 254 related to the Messinian Salinity Crisis, with the salt mobile unit dated between 5.97 and 5.33 Ma, and
12
13 255 earliest traces of the Messinian stage dated around 7.15 Ma (Karakitsios *et al.*, 2017).

15 256 We identify on the seismic dataset the contact between the Late Miocene Unit and the Messinian Event
16
17
18 257 according to the following criteria:

19
20 258 *-Late Miocene Unit:* During the Miocene, fluvial and floodplain deposits cover the North Aegean
21
22 259 Domain (Melinte-Dobrinescu *et al.*, 2009; Suc *et al.*, 2015). Drilling sites in the Prinos Basin that reach
23
24 260 Tortonian layers document an alternation of marine shales and turbidites in a distal marine environment,
25
26 261 followed by sandstone with marl and coal intercalations (Karakitsios *et al.*, 2017; Varesis & Anastasakis,
27
28 262 2021). On seismic data, the Late Miocene Unit is expressed by a series of interbedded channel systems
29
30 263 (Fig. 7).

31
32 264 *-Messinian Event:* The Messinian is dominantly expressed as an erosive surface in the North Aegean
33
34 265 Domain (Fig. 7), with a few evaporitic units scattered in some basins (e.g. Prinos; Mascle & Martin,
35
36 266 1990; Proedrou & Sidiropoulos, 1992; Proedrou & Papaconstantinou, 2004). Offshore Thermaïkos, the
37
38 267 thickness of the Messinian Unit displays important lateral variations, culminating at 0.8 s TWT (Varesis
39
40 268 & Anastasakis, 2021).

41
42
43 269

45 270 **4.2. Plio-Pleistocene Period**

46
47 271 The Pleistocene stratigraphy has mainly been constrained on the basis of sequence stratigraphy studies,
48
49 272 investigating the influence of sea level variations and oceanic current activity using the architecture of
50
51 273 sedimentary bodies (Sakellariou & Galanidou, 2017; Tripsanas *et al.*, 2016). In the North Aegean
52
53 274 Domain, sequence stratigraphy studies in the Thermaïkos Gulf (Lykousis, 2009) and offshore the Biga
54
55 275 Peninsula (Isler *et al.*, 2008) identified the reflectors corresponding to MIS (Marine Isotopic Stage) 2
56
57 276 (18 ka) to MIS 12 (430 ka). Additional stratigraphic constraints are obtained from the study of contourite
58
59 277 drifts in the Southern Aegean Domain since MIS 11 (420 ka), with an increased current intensity, and

1
2
3 278 hence, erosive events during interglacial periods (Tripsanas *et al.*, 2016). In the vicinity of the North
4
5 279 Aegean Trough, some coring document pro-delta formations during the Late Quaternary (last ~150 kyrs;
6
7 280 Piper & Perissoratis, 1991; Lykousis *et al.*, 2002).

8
9 281 Unfortunately, the published reports of the Prinos wells (Proedrou & Papaconstantinou, 2004) do not
10
11 282 provide stratigraphic details for the detritic Plio-Pleistocene sequence.

12
13 283 The only available stratigraphic constraints in the offshore Aegean Domain prior MIS12 are located at
14
15 284 the Myrtoon Basin (Anastasakis & Piper, 2005; Anastasakis *et al.*, 2006), which is about 250-km away
16
17 285 from our study area (Fig. 1). There, the age of the sedimentary layers is fairly well constrained as far as
18
19 286 2.8 Ma on the basis of correlation with DSDP Site 378 in the nearby Cretan Basin (Hsu *et al.*, 1978) and
20
21 287 the age of volcanic layers coming from Milos Island (Fytikas *et al.*, 1976, 1986; Anastasakis & Piper,
22
23 288 2005; Calvo *et al.*, 2012). This set of reflectors is also observed offshore the Evoikos Gulf (about 100
24
25 289 to 150 km away from our study area, Fig. 1) and their age is confirmed at 2 Ma upon the base of the sea-
26
27 290 level dependance of progradational packages of fluvial deposits (Anastasakis & Piper, 2013). However,
28
29 291 the Cycladic Plateau (Fig. 1, 7) has isolated the Myrtoon and Evoikos area (Fig. 1) from the North
30
31 292 Aegean Domain at various periods of sea-level lowstands (Sakellariou & Galanidou, 2017).

32
33 293 In order to investigate whether the stratigraphic constraints obtained at the Myrtoon Basin can be
34
35 294 correlated as far north as the North Aegean Domain, we compare a seismic-reflection profile collected
36
37 295 in the Myrtoon Basin (from Anastasakis & Piper, 2005) with a profile collected at the southern
38
39 296 termination of the Evia Basin, i.e. north of the Cycladic Plateau, here considered as the key feature of
40
41 297 the boundary between the north and south Aegean domains (Fig. 7). Despite a difference of resolution
42
43 298 between the two datasets, both profiles share similarities with respect to the seismic facies of the
44
45 299 Pliocene series up to a key reflector dated at 1.3 Ma (Fig.7).

46
47 300 Based on sequence stratigraphy studies and correlation with the Myrtoon Basin, we consider that four
48
49 301 Plio-Pleistocene key reflectors, corresponding to regional volcanic deposits and sapropel events
50
51 302 (Anastasakis & Piper, 2005), can be defined in the North Aegean Domain (fig. 7), separating four main
52
53 303 seismic units:

54
55
56
57 304 - *Reflector D* (2.8 Ma): In the wake of the Messinian event, numerous Gilbert deltas developed in the
58
59 305 surroundings of the Aegean Domain, followed by marine clastic sediments throughout the Pliocene,

1
2
3 306 characterized by distal channel systems (Proedrou & Papaconstantinou, 2004; Anastasakis & Piper,
4
5 307 2005). Anastasakis & Piper (2006) show the regional transition from terrestrial to full marine facies
6
7 308 occurred regionally at the boundary between the middle and upper Pliocene. A key reflector, labeled D,
8
9 309 seals the seismic unit interpreted as the episode of delta fan supply in the Aegean Sea (Fig. 7; Anastasakis
10
11 310 & Piper, 2005). This seismic unit is characterized by the signature of distal channel-levee systems,
12
13 311 marked by an alternation of minor downlap and onlap that reflects their successive avulsions. Reflector
14
15 312 D is the top reflector of a series of three high-amplitude reflectors sealing the systems of delta fans. The
16
17 313 reflector D is dated at ~2.8 Ma from Milos volcanics (Anastasakis & Piper, 2005).

18
19
20 314 - *Reflector C* (~2 Ma): Reflector C corresponds to an erosive surface, dated between 1.6 and 2.1 Ma
21
22 315 from the volcanic deposits related to the Oros eruption (Pe-Piper *et al.*, 1983; Dietrich *et al.*, 1988).
23
24 316 Sequence stratigraphy studies in the Evoikos Gulf suggest the age of reflector C to be closer to 2 Ma
25
26 317 than 1.6 Ma (a reflector distinct from C being dated at 1.6 Ma, Piper & Anastasakis, 2013).

27
28 318 -*Reflector B* (~1.3 Ma): Reflector B marks the onset of progradational wedges in the Aegean Sea, dated
29
30 319 around 1-1.4 Ma with lava flows (Anastasakis & Piper, 2005). The age has been refined at 1.3-1.4 Ma
31
32 320 from sequence stratigraphy studies in the Evoikos Gulf (Piper & Anastasakis, 2013).

33
34
35 321 -*Reflector A* (~430-480 ka): Reflector A is defined by a set of sequence stratigraphic constraints
36
37 322 available in the North Aegean Domain. It corresponds to MIS 12 (~430-480 ka). Our picking and spatial
38
39 323 correlation of reflector A in the North Aegean Trough agrees with the work of Ferentinos *et al.* (2018).

40
41 324

42 43 325 **5- RESULTS**

44 45 326 **5-1- Structure of the North Aegean Trough (Northern Branch of the North Anatolian Fault)**

46 47 327 5-1-1- The connection between the Gulf of Saros and the North Aegean Trough

48
49 328 At the northeastern entrance of the North Aegean Trough, the Main Splay of the North Anatolian fault
50
51 329 makes a bend, which is expressed on the seafloor by a series of push-up ridges (Fig. 3-4). The Main
52
53 330 Splay forms a steep, ~5 to 10° slope, which is covered by an undulated seafloor. There, a set of secondary
54
55 331 fault splays connects along the main fault. A 15-km-long ridge, referred to as the Medusa High (Masclé
56
57 332 & Martin, 1990; Sakellariou *et al.*, 2018), runs parallel to the North Anatolian Fault in the area of
58
59
60

1
2
3 333 bending (Fig. 3-4). A second splay, referred to as the Athos Splay, runs at 40° with respect to the North
4
5 334 Anatolian Fault and terminates at the tip of the Athos Peninsula (Fig. 3-4).
6
7 335 Seismic line 701 is perpendicular to the Athos splay (Fig. 8) and seismic line 702 crosses the area
8
9 336 between the main splay and the Medusa High (Fig. 9). The Main Splay runs across an area of chaotic
10
11 337 reflectors and forms a flower structure. The Athos Splay is an apparent normal fault dipping at 55°
12
13 338 southward, consistent with focal mechanisms at this location (Kiratzi & Louvari, 2003). The footwall
14
15 339 reveals a buried tilted block (Fig. 8). A dense network of normal faults, most of them being blind on the
16
17 340 seafloor, connects into a set of three flower structures in the basin, located at the footwall of the Athos
18
19 341 Splay (Fig. 8). The Medusa High (Fig. 9) corresponds to an elongated push-up structure (Masclé &
20
21 342 Martin, 1990; Sakellariou *et al.*, 2018).
22
23
24 343

26 344 5-1-2- The central segment of the North Aegean Trough offshore the Chalkidiki Peninsula

28 345 The Main Splay of the North Anatolian Fault runs within a 40-km-long, 15-km-wide, asymmetric
29
30 346 spindle-shaped trough (Fig. 3-4). Focal mechanisms confirm the strike-slip motion along the strike of
31
32 347 the Main Splay and suggest a minor component of transtension locally (Kiratzi & Louvari, 2003;
33
34 348 Kourouklas *et al.*, 2022). The Main Splay is sub-vertical and blind on the seafloor due to mass-wasting
35
36 349 sedimentation rates higher than its vertical slip-rate (~0.4-s TWT -thick package of mass transport
37
38 350 deposits on Line 603; Fig. 11). It forms a growth-synform structure on Line 602 (Fig. 10) and promotes
39
40 351 the uplift of the basement on line 603 (Fig. 11). The sedimentary cover of both flanks of the spindle-
41
42 352 shape basin displays an undulated configuration upslope, which becomes more chaotic downslope.
43
44 353 The Sithonia Splay is a second strike-slip fault trending 60°NE. To the west, a network of normal faults,
45
46 354 dipping 20° to the North, roots diagonally to the Sithonia Splay and forms a horsetail structure offshore
47
48 355 the Kassandra Peninsula, where focal mechanisms indicate normal faulting (Kourouklas *et al.*, 2022).
49
50 356 The multibeam map reveals two sedimentary basins along the Sithonia Splay: a first one, located on the
51
52 357 southern flank of the eastern segment of the fault and a second one, located on the northern flank of the
53
54 358 western segment of the fault (Fig. 5). The Sithonia Splay is subvertical in its central part, forming a
55
56 359 short-wavelength, symmetric growth-synform structure on Line 602 (Fig. 10). Line 603 indicates a
57
58 360 strong component of subsidence with a well-marked fanning of the sediments on the northern side of
59
60

1
2
3 361 the Sithonia Splay (Fig. 11). The westward increase of the subsidence corresponds to the transition
4
5 362 toward the transtensional regime of the horsetail termination (Fig. 5).

6
7 363 The Main Splay of the North Anatolian Fault and the Sithonia Splay are separated by a Central Structural
8
9 364 High (Fig. 3-4). The Central Structural High is a ~50-km-long elongated feature, with two highs
10
11 365 culminating at 700-m and 550-m depth. The Central Structural High appears as an antiform structure,
12
13 366 with undulations in the sedimentary cover (Fig. 10-11). The part of the antiform which is still exposed
14
15 367 at the seafloor corresponds to a basement high. A field of apparent normal faults with short and uneven
16
17 368 offsets is observed between the Central Structural High and the Sithonia Splay (Fig.10-11).

19
20 369

21
22 370 *5-1-3- Termination of the horsetail in the Thermaïkos-Skopelos area*

23
24 371 Offshore Skopelos, the geometry of the Main Splay of the North Anatolian Fault changes from a strike-
25
26 372 slip fault to a low-angle normal fault (Fig. 3-4), which runs along Pelion and the Thermaïkos Gulf
27
28 373 (Laigle *et al.*, 2000). The seismic reflection profile 103 (Fig. 12) crosses all the splays from Skopelos
29
30 374 Island to Kassandra Peninsula. We observe a large-scale rollover structure in the hanging wall of the
31
32 375 North Anatolian Fault, bending along the Main Splay, acting here as a north-dipping low-angle (~20°)
33
34 376 normal fault. Focal mechanisms however indicate pure strike-slip motion in this area (Kourouklas *et al.*,
35
36 377 2022), which suggests that the normal fault is turning into a strike-slip fault. The configuration of the
37
38 378 low-angle normal fault isolates a 20-km long, 10-km-wide trough along the Main Splay, filled-in by
39
40 379 mass transport deposits (Fig. 12). The hinge of the rollover is dissected by numerous synthetic and
41
42 380 antithetic normal faults. These fault systems cross a field of coalescing circular depressions spreading
43
44 381 over ~200-km², which corresponds to a series of short-wavelength undulated reflectors on the seismic,
45
46 382 focused on the uppermost ~0.4 s TWT (Fig. 12). The field of circular depressions is interpreted as the
47
48 383 result of fluid escape (Fig. 3-4).

49
50
51 384 The Central Splay (Fig. 3-4), roots on the Central Structural High, then bends across the extrados of the
52
53 385 rollover into a 25-km-long, 15-km-wide, 1450-m-deep trough, formed by a system of normal faults. The
54
55 386 normal fault scarps reach 350-m-high at the seafloor along the slope of the Gulf of Thermaïkos and
56
57 387 localize a system of slope-apron canyons.

1
2
3 388 The seismic line 201 (Fig. 13) crosses the area between the major low-angle ($\sim 35^\circ$ dip) normal fault
4
5 389 where the North Anatolian Fault ends and the termination of the Sithonia Splay. The hanging wall forms
6
7 390 a syncline basin, filled-in by sediments characterized by the short-wavelength undulated facies formed
8
9 391 by fluid escape. The system of normal faults crossing the slope of the Gulf of Thermaïkos forms a series
10
11 392 of horst and graben (Fig. 13). The termination of the Sithonia Splay is a set of two sub-parallel listric
12
13 393 faults, dipping 20° to 30° to the north, with their associated rollover structures dissected by synthetic
14
15 394 and antithetic normal faults (Fig. 13), consistent with the focal mechanisms at this location (Kourouklas
16
17 395 *et al.*, 2022).

18 396

19 20 21 22 397 **5-2-Structure of the Edremit-Skyros Trough (Southern Branch of the North Anatolian Fault)**

23
24 398 The structure of the Edremit-Skyros horsetail is described in details in Papanikoalou *et al.* (2019). In
25
26 399 this study, we present three new seismic profiles, which cross all the key structures of the Edremit-
27
28 400 Skyros Trough.

29
30 401 The seismic profile 801 (Fig. 14) crosses the Venus plateau, an oblique splay of the horsetail, the deepest
31
32 402 basin of the trough, here expressed as a growth syncline, and the main system of sub-parallel low-angle
33
34 403 ($\sim 25^\circ$ dip) normal faults bounding the Skyros Island, which isolates a half-graben. The seismic line 802
35
36 404 (Fig 15) crosses the southern branch of the North Anatolian Fault and the southern edge of the Edremit-
37
38 405 Skyros Trough. It reveals a series of angular unconformities associated to tilted blocks. On the seismic
39
40 406 profile 803 (Fig. 16), the oblique splays of the horsetail appear as normal faults isolating either half-
41
42 407 grabens or growth synclines, dominantly filled-in by mass transport deposits. The subsidence increases
43
44 408 towards the Skyros Island. Normal faults segment the bulge of the growth-synclines. In this area,
45
46 409 sedimentation rates exceed the vertical slip-rate at the faults, resulting in their smooth aspect on the
47
48 410 seafloor.

49 411

50 51 52 53 412 **5-3- Structure of the Evia Basin**

54
55 413 The Evia basin consists in a 90-km-long series of three subsiding basins, up to 1000-m deep, separated
56
57 414 by structural highs (Fig 3-4). On the seismic lines (Fig 17), all the Evia sub-basins appear as a series of
58
59 415 tilted half grabens bounded by a major normal fault on their SW flank. The maximum thickness of the

1
2
3 416 post-Messinian sediments reaches ~1 s (TWT). The series emplaced before the formation of the structure
4
5 417 display seismic facies typical of distal detritic sedimentation, while the syn-tectonic series display a
6
7 418 fanning configuration recording the progressive subsidence of the structure. Only minor Mass Transport
8
9 419 Deposits are observed within the growth structures, which results from the ~20° steep slope formed by
10
11 420 the main normal fault that does not allow the storage of sediments. The structural thresholds appear as
12
13 421 positive flower structures in line with the trend of the North Anatolian Fault, with uplifted segments of
14
15 422 the basement and a dense pattern of faults on their flanks.
16
17
18 423

20 424 **5-4- A diffuse fault system buried in the offshore North Aegean Domain**

21
22 425 The seismic lines collected during the NAFAS cruise in 2017 together with the compilation of vintage
23
24 426 seismic lines (Masclé & Martin, 1990; Beniest *et al.*, 2016) reveal fossil structures buried under the
25
26 427 sediments of the North Aegean Domain and locally crosscut by the horsetail structures.
27

28 428 The first structure is encountered in the area of the connection between the Saros Gulf and the North
29
30 429 Aegean Trough, at the -W-E trending Athos splay (Fig 3-4). There, the seismic line 701 (Fig 8) reveals
31
32 430 a buried tilted block sealed by a series of onlap terminations of the sedimentary layers.
33

34 431 The second structure also corresponds to a tilted graben, located at the plateau isolated between the
35
36 432 North Aegean Trough and the Edremit-Skyros Trough (Fig. 18). This graben is referred to as the Venus
37
38 433 graben.
39
40

41 434

43 435 **5-5- Chronology of tectonic events in the North Aegean Sea**

44
45 436 The series of angular unconformities labeled from A to D records the main tectonic events that shaped
46
47 437 the North Aegean Domain since the Messinian (Fig 7).
48

49 438 **5-5-1. The North Aegean Trough**

50
51 439 Unconformity D, dated at 2.8 Ma, records the end of the tectonic episode expressed by the series of
52
53 440 tilted blocks composed of the Athos (Fig. 8) and Venus (Fig. 18) grabens. This unconformity also marks
54
55 441 the deactivation of a series of push-up structures located in the area of the Central Structural High (line
56
57 442 603, Fig 11). At the termination of the Sithonia Splay (line 201, Fig 13) offshore Kassandra Peninsula,
58
59
60

1
2
3 443 this unconformity marks the onset of a fanning configuration of the sediments and, therefore, the onset
4
5 444 of the tilt of the graben.

6
7 445 The second key angular unconformity C, dated at 2 Ma, is well identified by onlap terminations over
8
9 446 the underlying, tilted deposits in the North Aegean Trough (e.g. in the vicinity of Skopelos at line 103,
10
11 447 Fig 12). This unconformity marks the onset of the fanning configuration of the sediments observed all
12
13 448 along the Sithonia Splay (line 201, Fig 13; line 602-603, Fig 10-11), and hence, the formation of this
14
15 449 still-active splay within the North Aegean Trough. The amplitude of slope incision features remains
16
17 450 poorly disturbed by this tectonic episode (e.g. at the edge of the Thermaikos Gulf, line 201, Fig 13),
18
19 451 which indicates a still rather low subsidence rate.

20
21
22 452 These unconformities D and C record the Late Pliocene-Early Pleistocene change in the pattern of strain
23
24 453 localization within the North Anatolian Shear Zone. These unconformities also pre-date the first stage
25
26 454 of the formation of the North Aegean horsetail structure, with the activation of the Sithonia Splay.

27
28 455 The third angular unconformity B, dated at ~1.3 Ma, records the formation of the termination of the
29
30 456 central splay (observed at line 103, Fig 12). Across the edge of the Thermaikos Gulf, the 1.3 Myrs-old
31
32 457 unconformity corresponds to an increase in the amplitude of the slope incisions features (line 201, Fig
33
34 458 13), which indicates a major increase in the overall subsidence, the channels digging deeper to catch
35
36 459 their equilibrium line. The Mass Transport Deposits associated to this episode are the thickest (~0.2-0.3
37
38 460 s TWT) encountered within the North Aegean Domain since the Messinian. At the connection between
39
40 461 the North Aegean Trough and the Saros Gulf, the 1.3 Myrs-old unconformity records the formation of
41
42 462 the Athos Splay and the main uplift of the Medusa High (Fig 8-9). There, the mean vertical slip-rate of
43
44 463 the Athos normal fault increased from a 0.13 mm.yr^{-1} during the 2-1.3 Ma interval to 0.22 mm.yr^{-1} since
45
46 464 1.3 Ma. Overall, this set of observations indicates a major structural reorganization of the northern
47
48 465 branch of the North Anatolian Fault at 1.3 Ma, marked by a drastic increase in subsidence rates within
49
50 466 the sub-basins of the North Aegean Trough.

51
52
53 467 Finally, unconformity A, dated at ~0.5 Ma, records the onset of the Main Splay of the North Anatolian
54
55 468 Fault all across the North Aegean Trough (Ferentinos *et al.*, 2018). The formation of the Main Splay is
56
57 469 best recorded offshore Skopelos (line 103, Fig 12), the segment of the fault running at the edge of the
58
59 470 Central High being affected by current and gravity-driven erosion (line 602, Fig 10). The activation of

1
2
3 471 the Main Splay induced a change in the activity of the Sithonia Fault, with an increase of the vertical
4
5 472 slip-rate from 0.16 mm.yr⁻¹ during the 1.3-0.48 Ma interval to 0.3 mm.yr⁻¹ since 0.48 Ma. However, the
6
7 473 vertical slip-rate of the faults related to the Central Splay remained steady.
8

9 474

11 475 5-5-2. The Skyros-Edremit Trough

13 476 The unconformity C (2 Ma) is overlapped by a tilted series of reflectors on the southern edge of the trough
14
15 477 (line 803, Fig. 16). This unconformity marks the first stages of the formation of the Southern branch of
16
17 478 the North Anatolian Fault offshore Skyros. Unconformity B (1.3 Ma) corresponds to the increase in the
18
19 479 subsidence rate (up to 0.45 mm.yr⁻¹) at the hanging wall of the normal fault system running along Skyros
20
21 480 Island (Fig. 14, 15, 16). Unconformity A (~0.5 Ma) is well expressed close to the oblique splay 1 and
22
23 481 marks an increase in subsidence at the hanging wall of this splay (Fig. 15). Unconformity A therefore
24
25 482 records the formation of the oblique splay 1 (Fig. 16).
26
27

28 483

30 484 5-5-3. The Evia basin

32 485 The onset of subsidence within the Evia Basin is dated between 2 and 1.3 Ma based on unconformities
33
34 486 B and C (Fig. 17). This marks the base of the fanning configuration of the sedimentary infill. The main
35
36 487 formation episode of the Evia Basins is therefore coeval with the increase in subsidence at Corinth and
37
38 488 the first step of strain localization at both the northern and southern branches of the North Anatolian
39
40 489 Fault.
41
42

43 490

45 491 6- Discussion

47 492 The present-day configuration of the North Aegean Domain shows the gradual kinematic transition from
48
49 493 the strike-slip deformation that dominates in the northeastern Aegean Domain to the dip-slip
50
51 494 deformation encountered in the Northwest Aegean Domain (Mouslopoulou *et al.*, 2007a,b). Our new
52
53 495 set of geological constraints allows us to refine the framework of strain localization of the North
54
55 496 Anatolian Shear Zone in the North Aegean Domain and highlights the westward propagation of the
56
57 497 strike-slip dominated area since the Late Miocene. The new geological constraints obtained from the
58
59
60

1
2
3 498 seismic-reflection dataset are summarized in Figure 19 and integrated to the previously available
4
5 499 constraints on the geological events of the area.
6

7 500

9 501 6-1. Mode of formation of horsetail structures: the North Aegean and Edremit-Skyros Troughs

11 502 The formation of the horsetail terminations of both the northern and southern branches of the North
12
13 503 Anatolian Fault occurs in the frame of the westward propagation of the North Anatolian Fault within
14
15 504 the prevailing NNE-SSW to N-S extensional conditions of the western North Aegean Domain. The
16
17 505 horsetail configuration emplaces where the strike-slip fault connects a system of low-angle normal faults
18
19 506 inherited from the extensive stage.

21
22 507 The North Aegean and the Edremit-Skyros Troughs are horsetail terminations that are currently at
23
24 508 different steps of their development. Although the formation of both structures initiated at the same age
25
26 509 (~2 Ma), the lower slip rate along the southern branch of the North Anatolian Fault leads the Edremit-
27
28 510 Skyros to be structurally less mature. This differential stage of horsetail structural evolution allows us
29
30 511 to investigate the tectonic and sedimentary processes at their origin.

32 512 On one hand, the Edremit-Skyros Trough corresponds to the evolution of a single horsetail structure.
33
34 513 The oblique splays of the Edremit-Skyros Trough formed first along the main detachment fault, then
35
36 514 migrated eastwards (oblique splay 1 formed at 0.5 Ma).

38 515 On the other hand, the North Aegean Trough consists in three horsetail basins (at the end of the Sithonia,
39
40 516 Central and Main Splays) that merged in a single one. Our seismic dataset highlights the successive
41
42 517 activation of the Sithonia Splay at 2 Ma, the Central Splay at 1.3 Ma and the Main Splay at 0.5 Ma,
43
44 518 which corresponds to the westward propagation of the northern branch of the North Anatolian Fault (Fig
45
46 519 18). The distance between the negative flower structure at the end of each splay is on the order of 30 to
47
48 520 50-km. This corresponds to the distance added to the northern branch of the North Anatolian Fault every
49
50 521 0.7-0.8 Ma in the frame of its westward propagation. The three main splays of the North Aegean Trough
51
52 522 have remained active since their inception. The decrease in slip rates observed in GPS measurements at
53
54 523 the Sporadhes Archipelago (Müller *et al.*, 2013) may be the result of slip partitioning over each major
55
56 524 splay of the North Aegean Trough (Fig. 1).
57
58
59
60

1
2
3 525 This framework of structural evolution of the horsetail terminations encountered in the North Aegean
4
5 526 Domain provides a ground-truth validation of analog modeling tests performed by Basile & Brun (1999).
6
7 527 In their models (Fig 20), a horsetail termination initially consists in an en-échelon normal fault system
8
9 528 trending perpendicular to the main strike-slip displacement zone, composed of oblique Riedel splays.
10
11 529 As the relative motion between the adjacent blocks increases, the Riedel splays progressively connects
12
13 530 the en-échelon normal fault system. For dextral motion, the first Riedel fault forms to the east of the
14
15 531 horsetail and the subsequent splays propagate westwards. Accordingly, the en-échelon normal faults are
16
17 532 first captured in the overall horsetail structure in the east. The western en-échelon normal faults are
18
19 533 progressively captured within the horsetail structure during its maturation. While some grabens
20
21 534 associated to the en-échelon normal faults are captured by the oblique splays, others are crosscut by the
22
23 535 propagating main displacement zone. Once initiated, all the oblique splays remain active during the
24
25 536 lifetime of the horsetail.
26
27
28
29

30 537
31 538 6-2. The Plio-Pleistocene transition from a wide North Anatolian Shear Zone to a localized North

32 539 Anatolian Fault

34 540 Our structural analysis further highlights the Late Pliocene change in stress regime (Lyberis, 1984) at
35
36 541 the scale of the North Aegean Domain (Fig. 21). From the Serravalian to the Late Pliocene, the North
37
38 542 Anatolian Shear Zone consisted in a diffuse system of en-échelon normal faults connected through
39
40 543 dextral transfer faults, thereby isolating a series of basins. These basins include a set of Late Miocene-
41
42 544 Early Pliocene basins compartmentalizing the Rhodope Core complex (Brun & Sokoutis, 2018) and the
43
44 545 series of basins identified at sea in the vicinity of the North Aegean Trough, including the Athos and
45
46 546 Venus grabens, deactivated at 2.8 Ma (Fig. 21a).

47
48
49 547 Our reconstructions at 2 and 1.3-0.8 Ma (Fig. 21b-c) show the period of transition from the wide shear
50
51 548 zone to the two main branches of the North Anatolian Fault; i.e. the period of effective propagation of
52
53 549 the North Anatolian Fault in the North Aegean Sea. This transition is roughly coeval with the
54
55 550 deactivation of the South Marmara Fault dated by Le Pichon *et al.* (2015) and the subsequent activation
56
57 551 of the Main Marmara Fault. While propagating westward, the strike-slip segments of the North
58
59 552 Anatolian Fault either connected or crosscut the Late Pliocene system of en-échelon grabens including

1
2
3 553 the Athos and Venus grabens. Unconformity C (Fig. 21c-d) records the first stage of formation of the
4
5 554 northern and southern branches of the North Anatolian Fault at the North Aegean Trough and the
6
7 555 Edremit-Skyros Trough, whereas unconformities B and A marks the successive steps of development
8
9 556 of these basins.

10
11 557 If we consider the series of Serravalian-Pliocene basins dissecting the Rhodope Core complex (Brun &
12
13 558 Sokoutis, 2018) as the earliest traces of the North Anatolian Shear Zone in the North Aegean Domain,
14
15 559 then the North Anatolian Shear Zone remained a diffuse transtensive system for about 5 to 7 Myrs until
16
17 560 the Messinian, with a first step of localization marked by the formation of the Ganos-Saros segment at
18
19 561 ~5 Ma (Armijo *et al.*, 1999). The Anatolia-Eurasia relative motion used to be distributed over this
20
21 562 transtensive system composed of multiple en-échelon fault segments prior to Messinian. The enhanced
22
23 563 localization of the North Anatolian Shear Zone in the North Aegean Domain evidenced here at 2-1.3
24
25 564 Ma coincides with the Early Pleistocene increase in slip-rates along the North Anatolian Fault (Hubert
26
27 565 Ferrari *et al.*, 2010). The localization of the North Anatolian Fault therefore contributed to the Early
28
29 566 Pleistocene change in stress regime recorded over the entire Aegean, previously attributed to a change
30
31 567 in the dynamics of the Hellenic Subduction Zone (Lyberis, 1984; Mascle & Martin, 1990; Armijo *et al.*,
32
33 568 1992; Sakellariou & Tsampouraki-Kraounaki, 2016).

34
35
36
37 569 In this frame, the ‘wide shear-stage’ of the North Anatolian Shear Zone and the diachronous strain
38
39 570 localization within it lasted several million years longer in the western North Aegean Domain than east
40
41 571 of the Yeniçaga Fork (Fig. 21; Sengör *et al.*, 2005). Some fault segments are localized since the
42
43 572 Messinian (e.g. the Ganos-Saros fault) while others formed in the Early Pleistocene (e.g. the North
44
45 573 Aegean and the Edremit-Skyros Troughs). This implies that some diffuse en-échelon systems (e.g.
46
47 574 Chalkidiki or Marmara at 3.5-4 Ma) remain active while major, several hundred-km-long localized fault
48
49 575 segments (e.g. Ganos-Saros segment) exist in between (Fig. 21). Further strain localization involved the
50
51 576 abandonment of Late Miocene-Early Pliocene en-échelon faults (e.g. Strymon, Drama, Prinos) and
52
53 577 major transfer strike-slip faults (e.g. transfer faults within the Thrace basin, the South Marmara Fault).

54
55
56 578

57
58 579 **7-Conclusions**

1
2
3 580 Our study documents multiple episodes of strain localization within the North Anatolian Shear Zone in
4
5 581 the North Aegean Domain. During the Late Serravalian to the Early Pliocene, the North Anatolian Shear
6
7 582 Zone was a diffuse transtensive fault zone. During the Late Pliocene, strike-slip strain localized along
8
9 583 some fault segments (e.g. the Ganos-Saros segment) while remained diffuse in others (Prinos, Strymon,
10
11 584 Drama, Thrace basins, Fig 21). Offshore sediments record the first abrupt step of strain localization
12
13 585 along the northern and southern branches of the North Anatolian Fault in the North Aegean Domain at
14
15 586 2-1.3 Ma. This is coeval with the general increase of slip rate along the entire North Anatolian system
16
17 587 and the regional change in stress regime over the Aegean Sea. Further westward propagation and
18
19 588 localization along the northern and southern branches formed the North Aegean and Skyros-Edremit
20
21 589 Troughs as horsetail structures. The North Aegean Trough results from the formation of three successive
22
23 590 horsetails, formed at 2 Ma, 1.3 Ma and 0.5 Ma and propagating westward at a rate of 40 to 60 km.Myr⁻¹.
24
25
26 591
27
28
29
30

31 **Acknowledgements:**

32
33 594 We warmly thank the crew members of the R/V Tethys II involved in the NAFAS cruise. This study
34
35 595 benefits from the support of INSU-CNRS (RHEOSTRIKE project). We warmly thank L. Jolivet and M.
36
37 596 Laigle for their precious support and helpful advices. We thank Dr. Vasiliki Mouslopoulou and an
38
39 597 anonymous reviewer for their highly constructive and helpful comments. We dedicate this study to the
40
41 598 memory of Pr. Jean-Pierre Brun, who supported and inspired us during the earliest stages of this project.
42
43
44

45 600 **Author's contributions:**

46
47 601 **Conception of the project** : M. Rodriguez; C. Gorini; D. Sakellariou; L. Lepourhiet; E. d'Acremont;
48
49 602 S. Arsenikos; F. Chanier; P. Briole

50
51 603 **NAFAS cruise organization, Data acquisition and processing** : M. Rodriguez; A. Janin; E.
52
53 604 d'Acremont; N. Chamot Rooke; K. Tsampouraki-Kraounaki ; I. Morfis; G. Rousakis; A. Lurin; M.
54
55 605 Delescluse; D. Oregioni ; J.-X. Dessa; A. Nercessian

56
57 606 **Multibeam acquisition and interpretation** : D. Sakellariou; I. Morfis; G. Rousakis; K. Tsampouraki
58
59 607 Karounaki ; M. Rodriguez
60

1
2
3 608 **Seismic interpretation** : M. Rodriguez; A. Janin; A. Lurin; C. Gorini; D. Sakellariou
4

5 609 **Geological expertise, integration of the results to the geological background**: M. Rodriguez; D.
6

7 610 Sakellariou; C. Gorini; P. Henry; C. Grall; A. Beniést; D. Fernandez Blanco; A. Rigo; C. Bulois; F.
8

9 611 Chanier; F. Caroir; L. Lepourhiet
10

11 612
12

13 613 **Data availability:**

14
15 614 Seismic reflexion dataset available on request to Dr. M. Rodriguez (rodriguez@geologie.ens.fr) and Dr
16

17
18 615 M. Delescluse (delescluse@geologie.ens.fr).
19

20 616 Multibeam dataset available on emodnet <https://emodnet.ec.europa.eu/en/bathymetry>
21

22 617
23

24 618
25

26 619
27

28 620
29

30 621
31

32 622
33

34 623
35

36 624
37

38 625
39

40 626
41

42 627
43

44 628
45

46 629
47

48 630
49

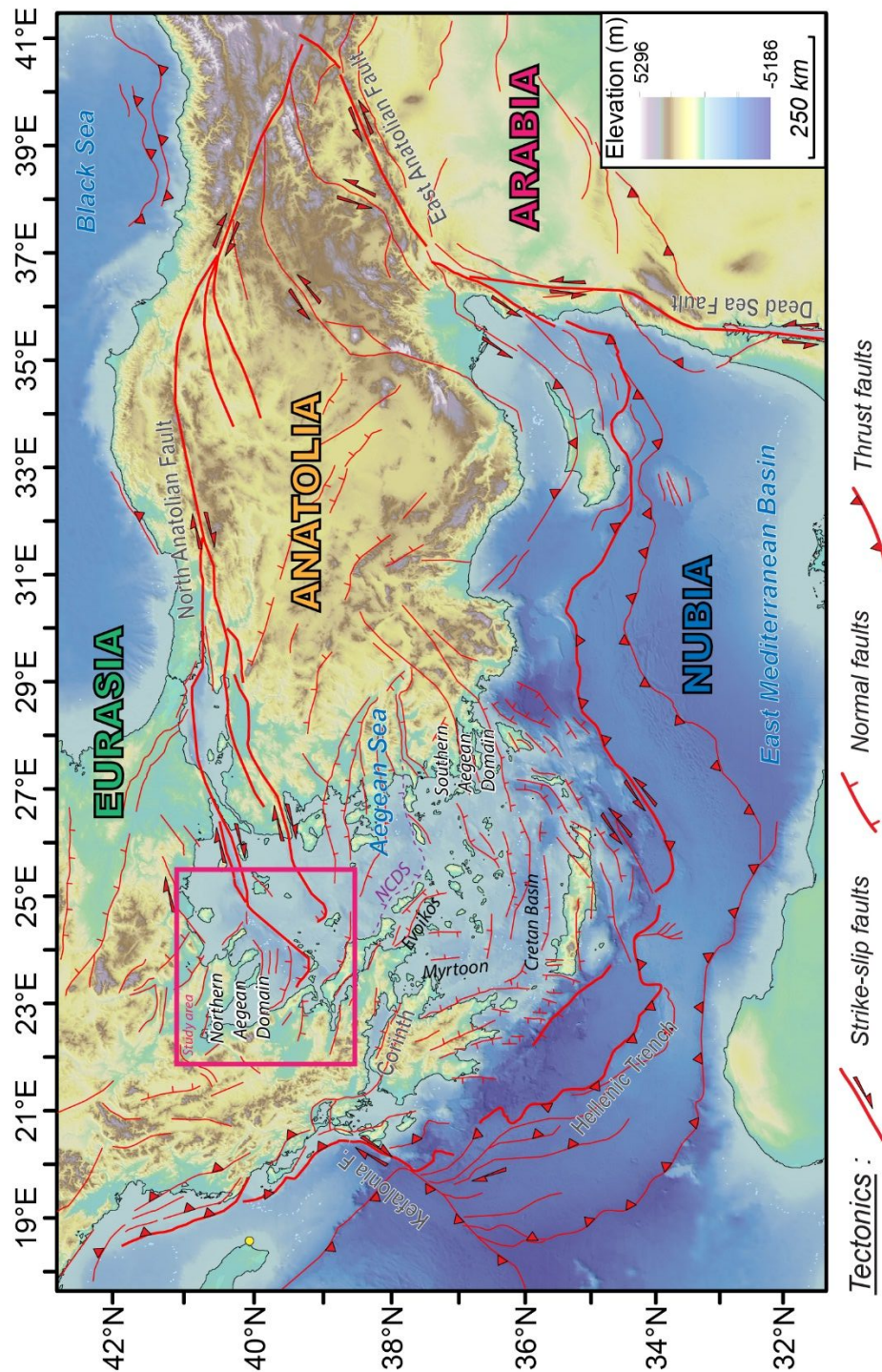
50 631
51

52 632
53

54 633
55

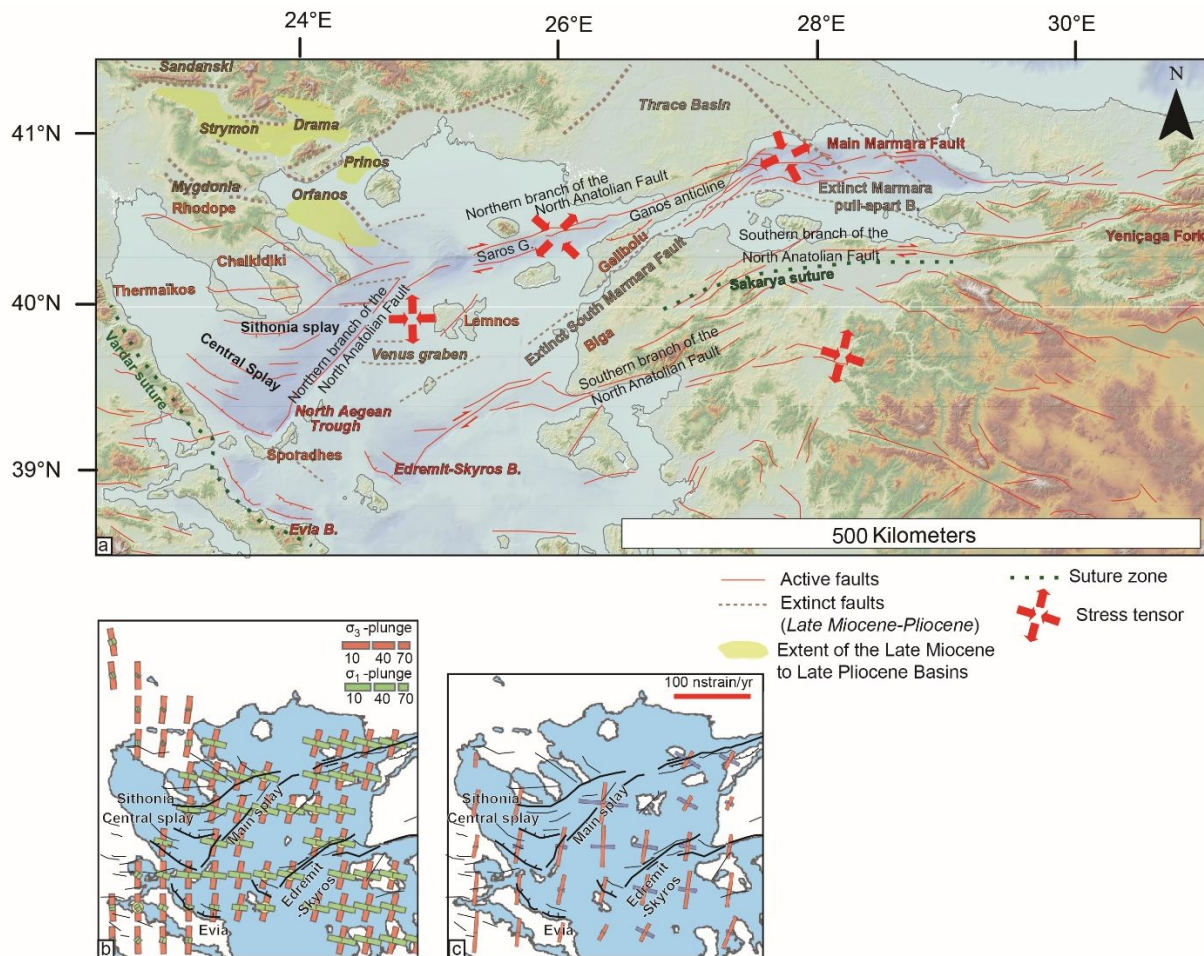
56 634
57

58 635
59
60

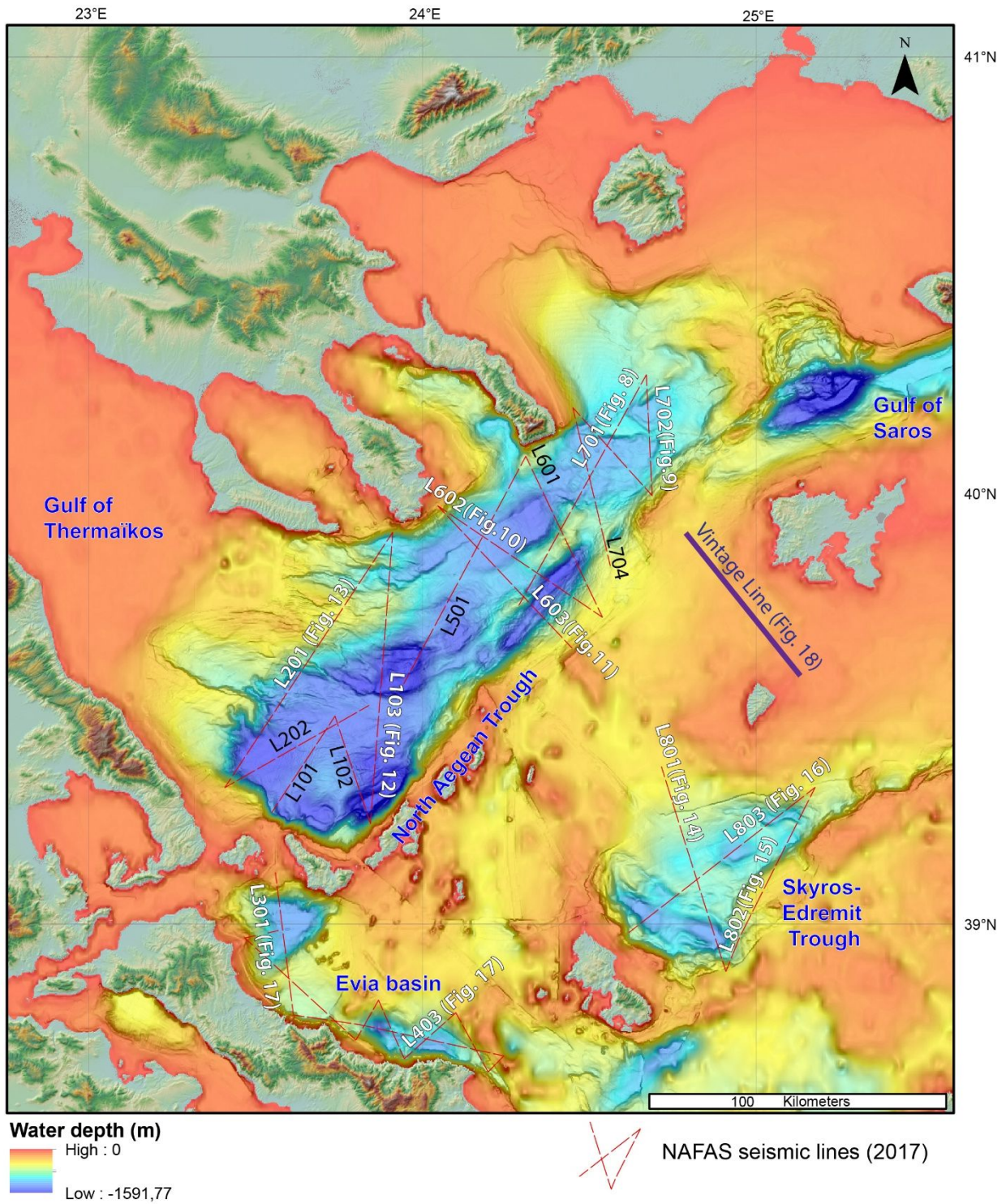
636 **Figures:**

637

638 **Figure 1:** Tectonic framework of the Eastern Mediterranean Sea (active faults from Kremer and
 639 Chamot-Rooke, 2004 and Chamot-Rooke et al., 2005). The tectonic escape of Anatolia results from
 640 interactions between Arabia-Eurasia and the Hellenic trench retreat. NCDS: North Cycladic Detachment
 641 System



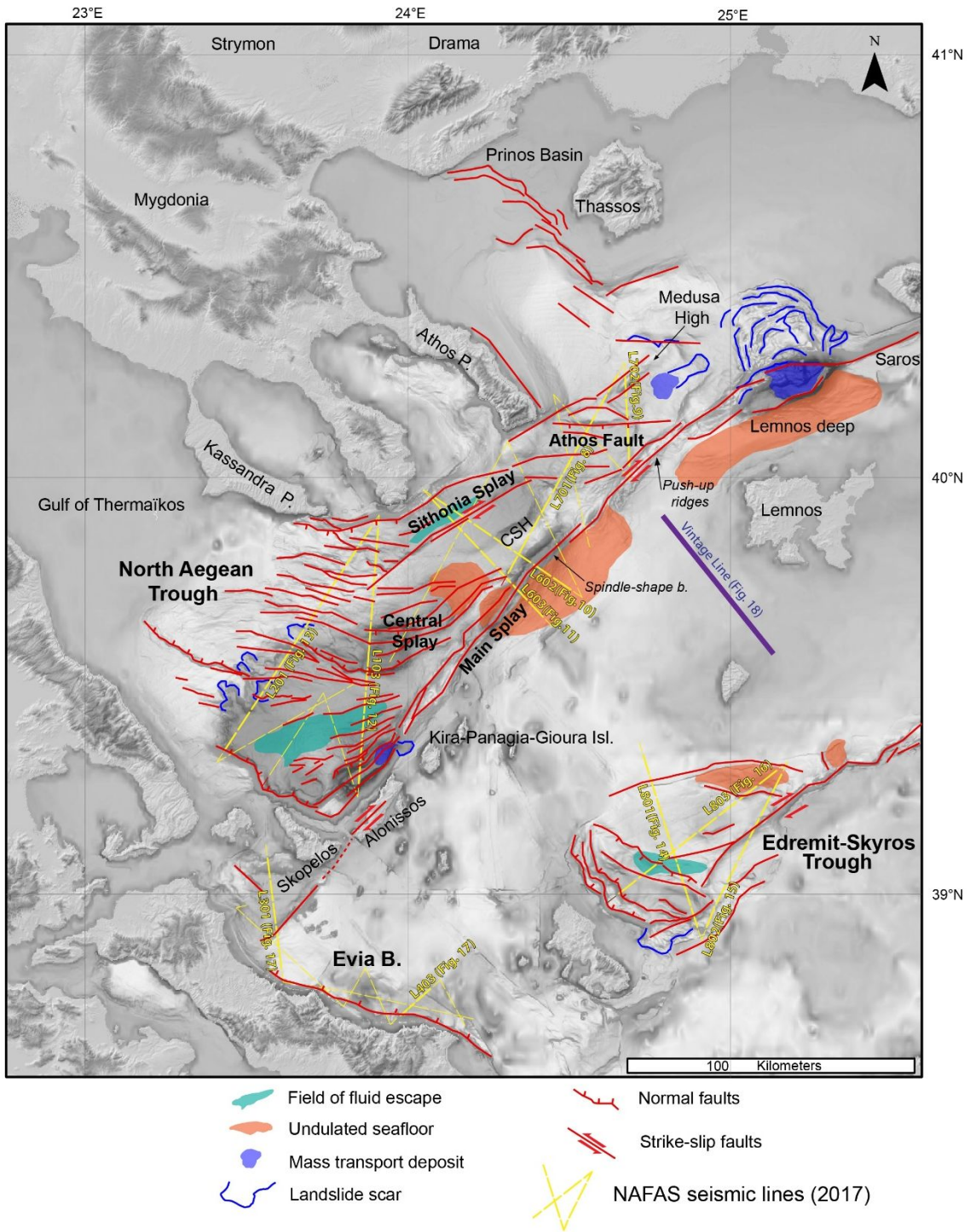
642
 643 **Figure 2:** a) Structural map of the segment of the North Anatolian Shear Zone in the North Aegean
 644 Domain, modified after Lyberis (1984), Koukouvelas and Aydin (2002), Yalçin et al. (2016);
 645 Sakellariou et al. (2018), Papanikolaou et al. (2002; 2019). The stress tensors are from Gürer et al.
 646 (2016); Sümer et al. (2018). The location of the Late Miocene-Late Pliocene basins (Strymon,
 647 Mygdonia, Drama, Orfanos, Prinos) is from Brun and Sokoutis (2018). b) Present-day stress tensors and
 648 c) strain rate, from Floyd et al. (2010) and Konstantinou et al. (2016).



649

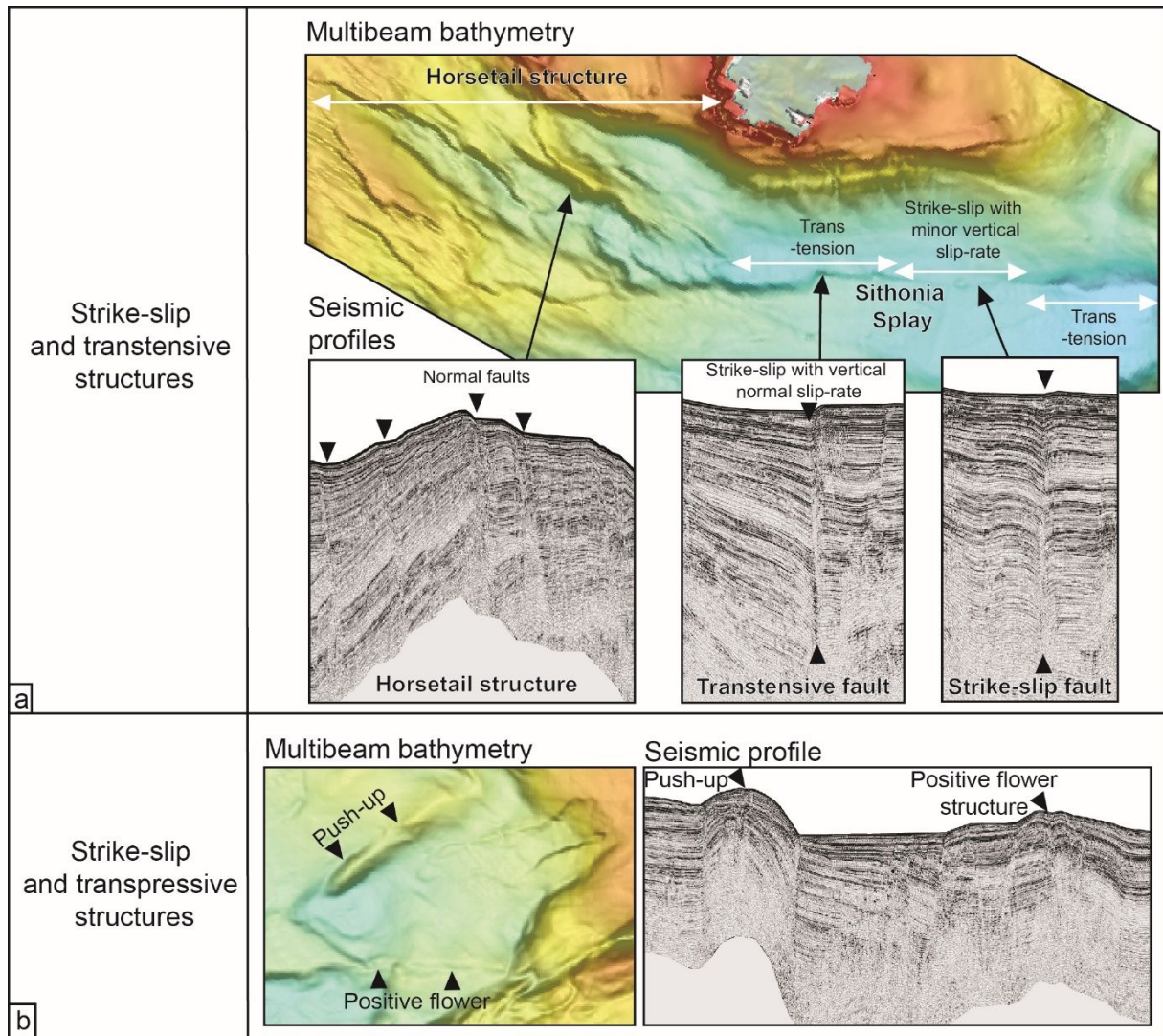
650 **Figure 3:** Topographic and bathymetric map of the North Aegean Domain and location of the seismic

651 lines published in this study (Sakellariou et al. 2018; Papanikolaou et al., 2002; 2019)



652

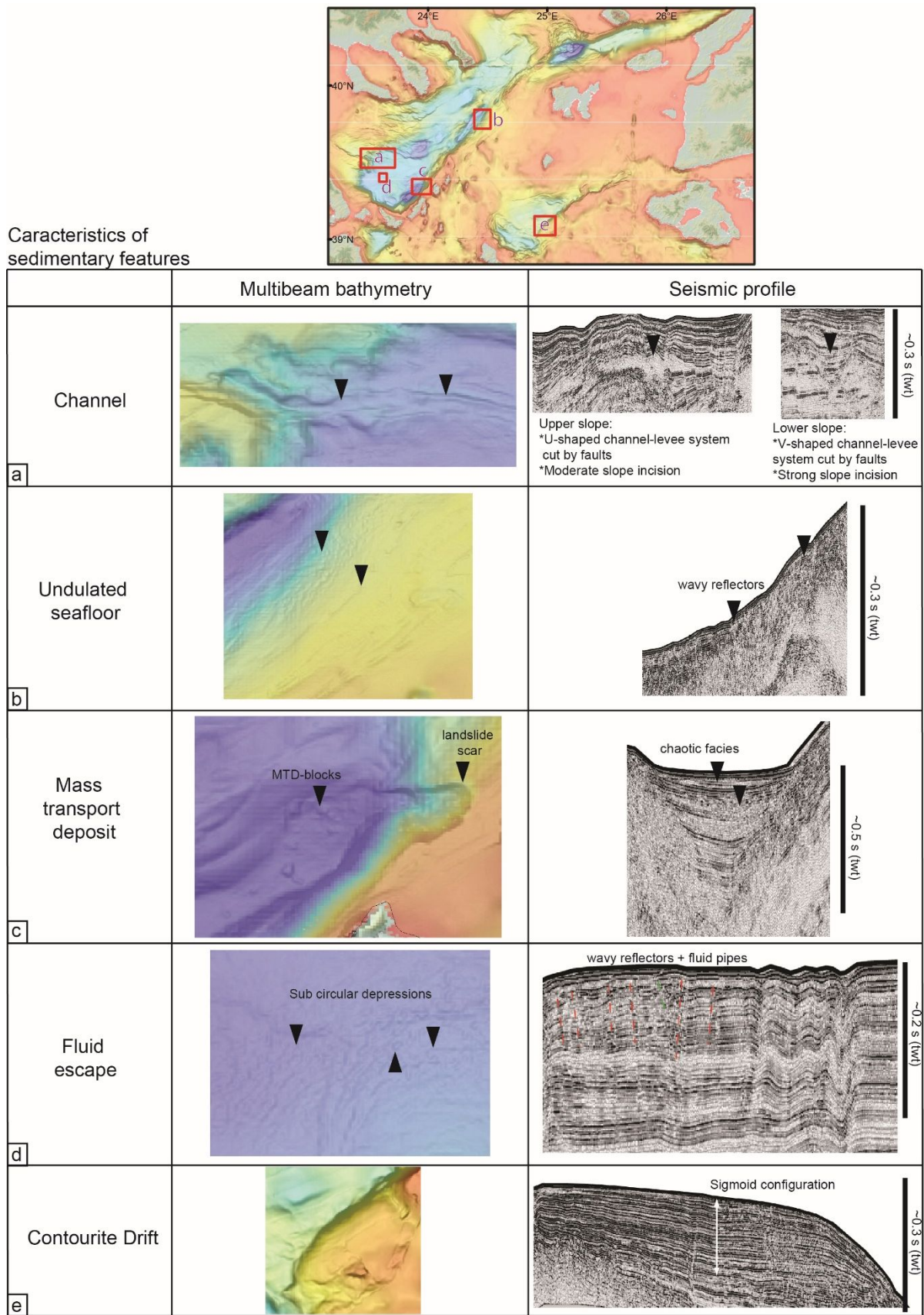
653 **Figure 4:** Structural map of the active faults of the North Aegean Trough and the Edremit-Skyros
 654 Trough and the main sedimentary features (modified after Sakellariou et al. 2018; Papanikolaou et al.,
 655 2002; 2019). CSH: Central Structural High



656

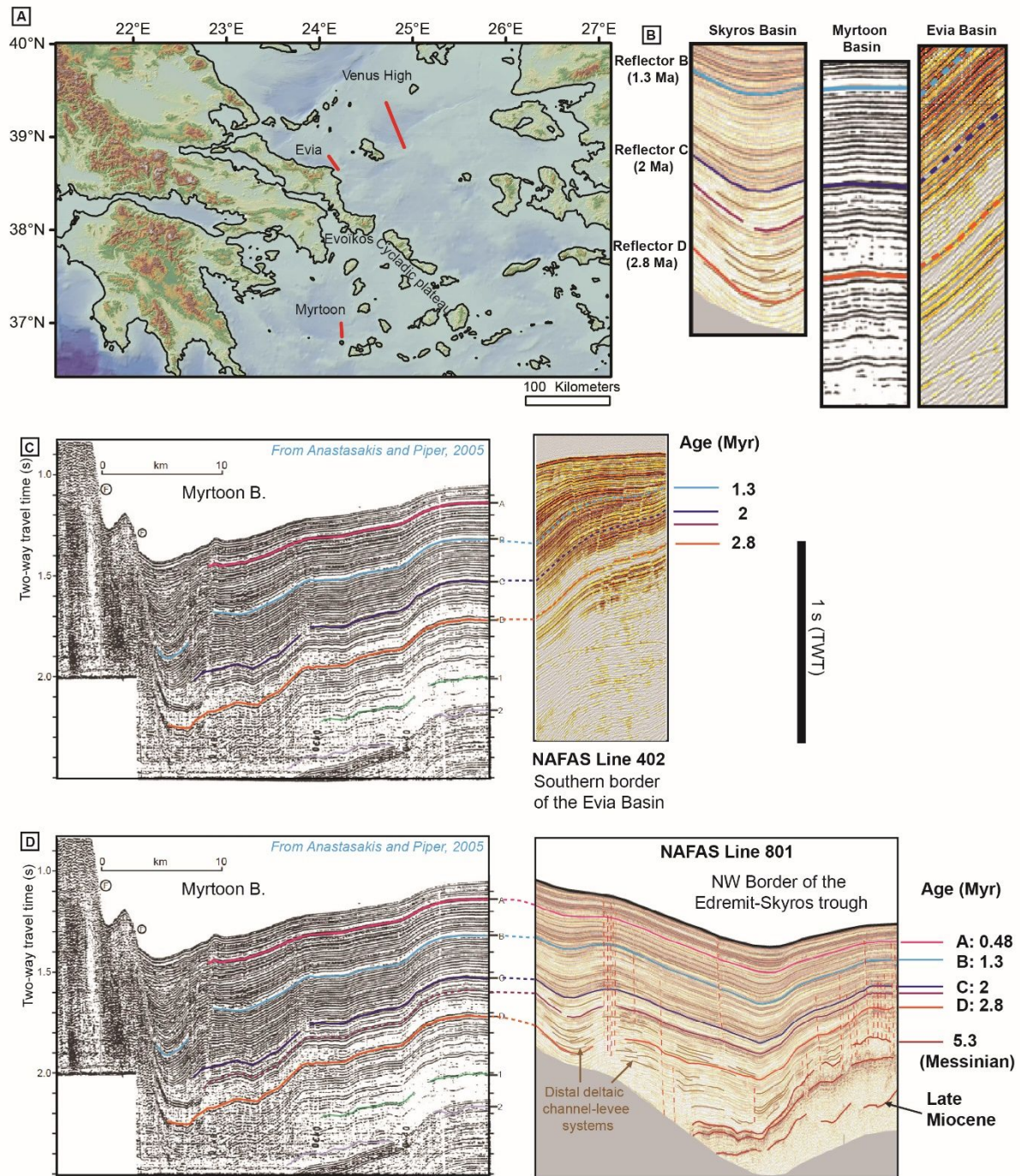
657

658 **Figure 5:** Criteria of identification of transtensive and transpressive strike-slip structures on the
 659 multibeam and seismic-reflection dataset, with the examples of a) the Sithonia Splay and b) the Athos
 660 Splay



661

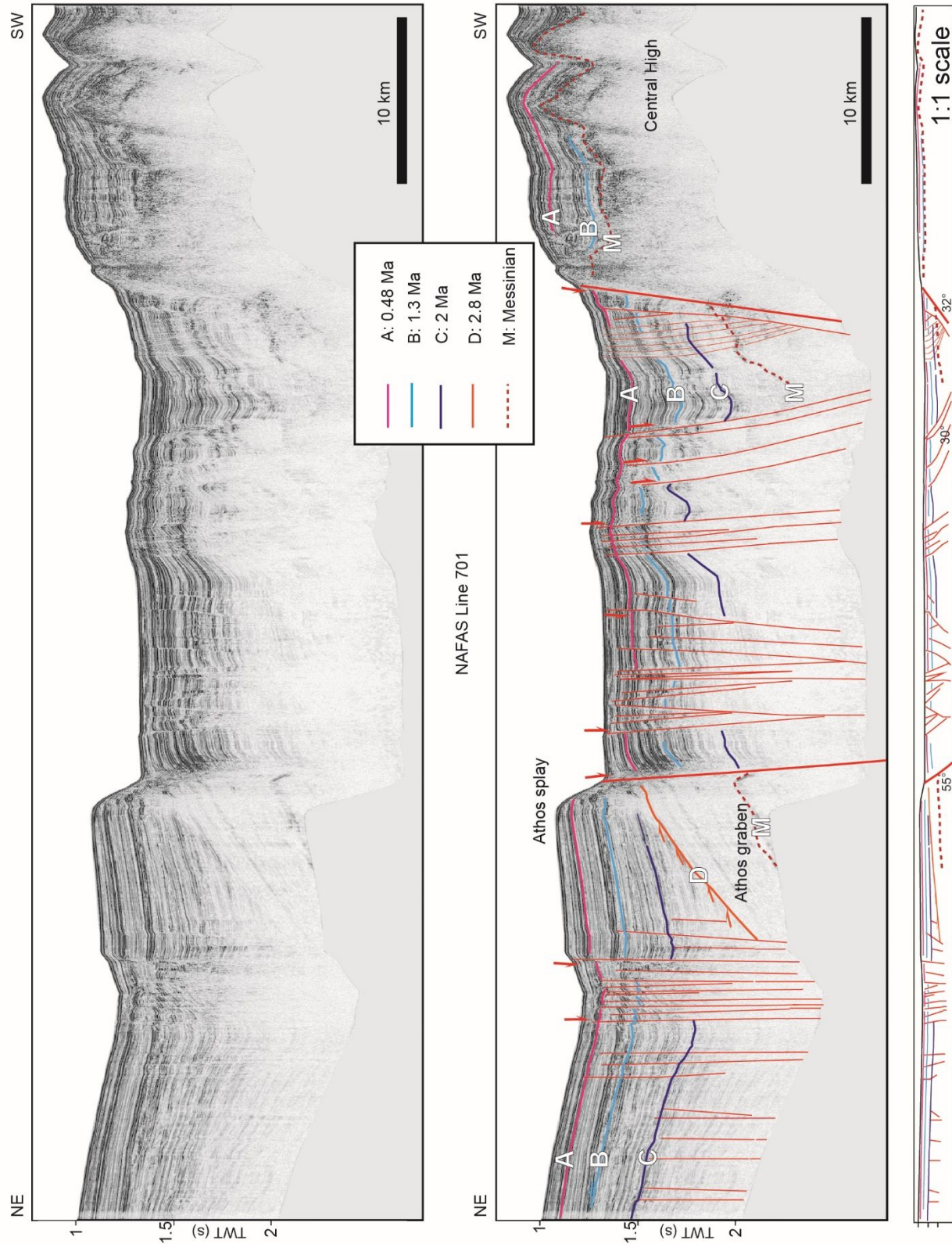
662 **Figure 6:** Classification of the facies of the main sedimentary features observed on the multibeam and
 663 seismic dataset in the study area



664

665 **Figure 7:** Stratigraphic correlation between the Myrtoon basin (Anastasakis and Piper, 2005), the Evia

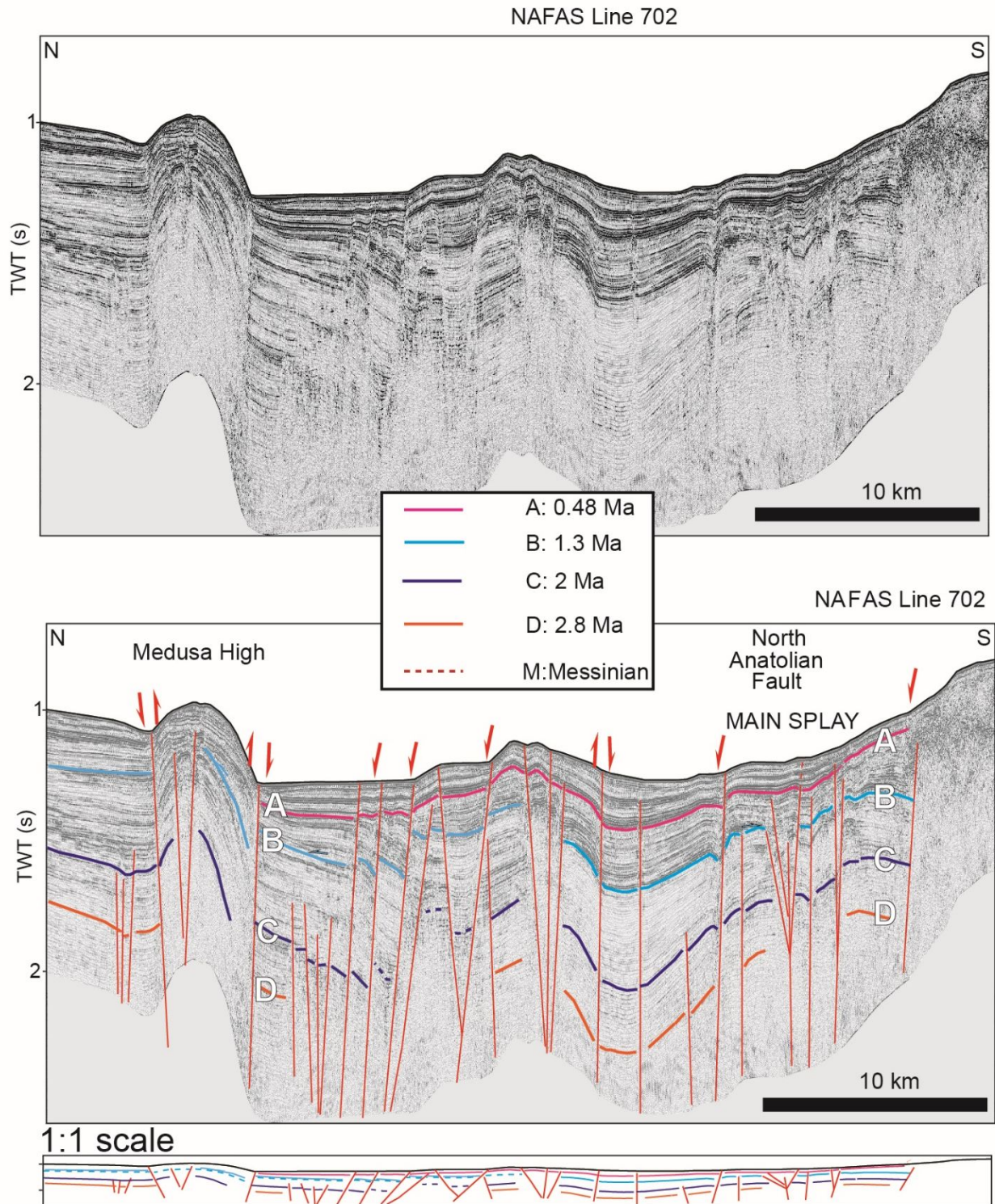
666 Basin and the NW border of the Edremit-Skyros Trough



667

668 **Figure 8:** Seismic line 701 from the NAFAS cruise, crossing the Athos Splay and the North Anatolian

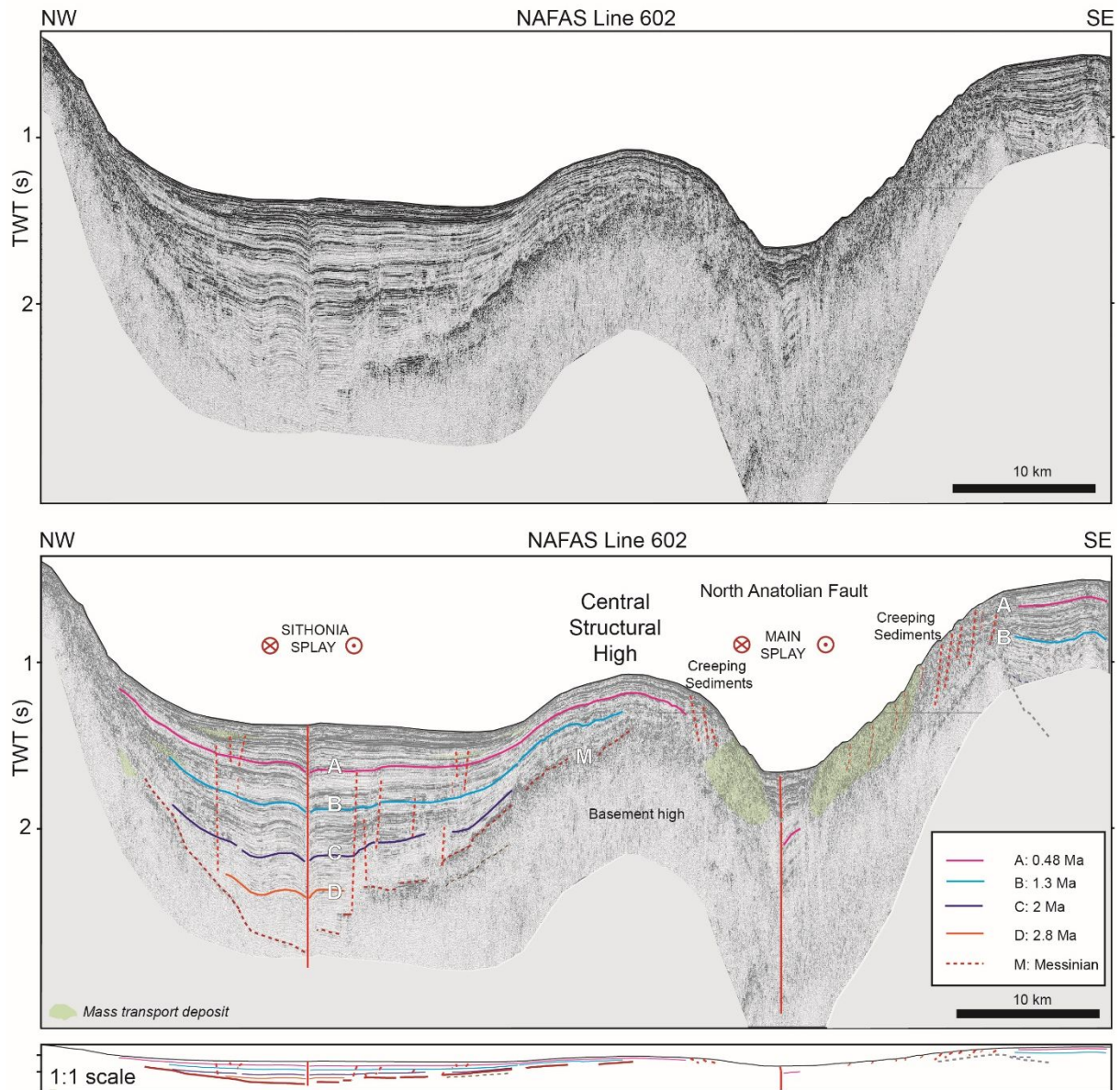
669 Fault at the entrance of the North Aegean Trough. See figure 3 for location.



670

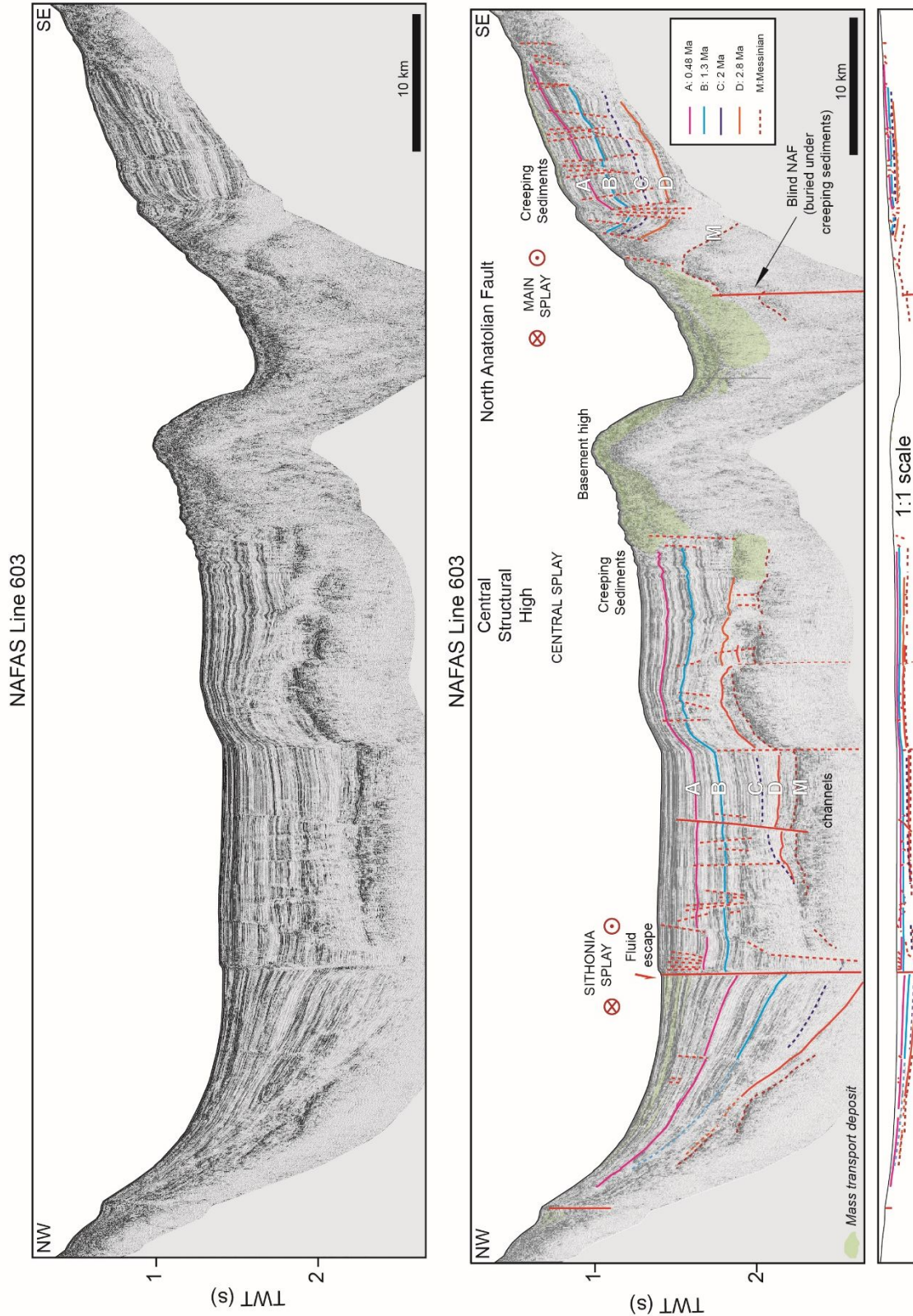
671 **Figure 9:** Seismic line 702 from the NAFAS cruise, crossing the Medusa High and the North Anatolian

672 Fault. See figure 3 for location.



673

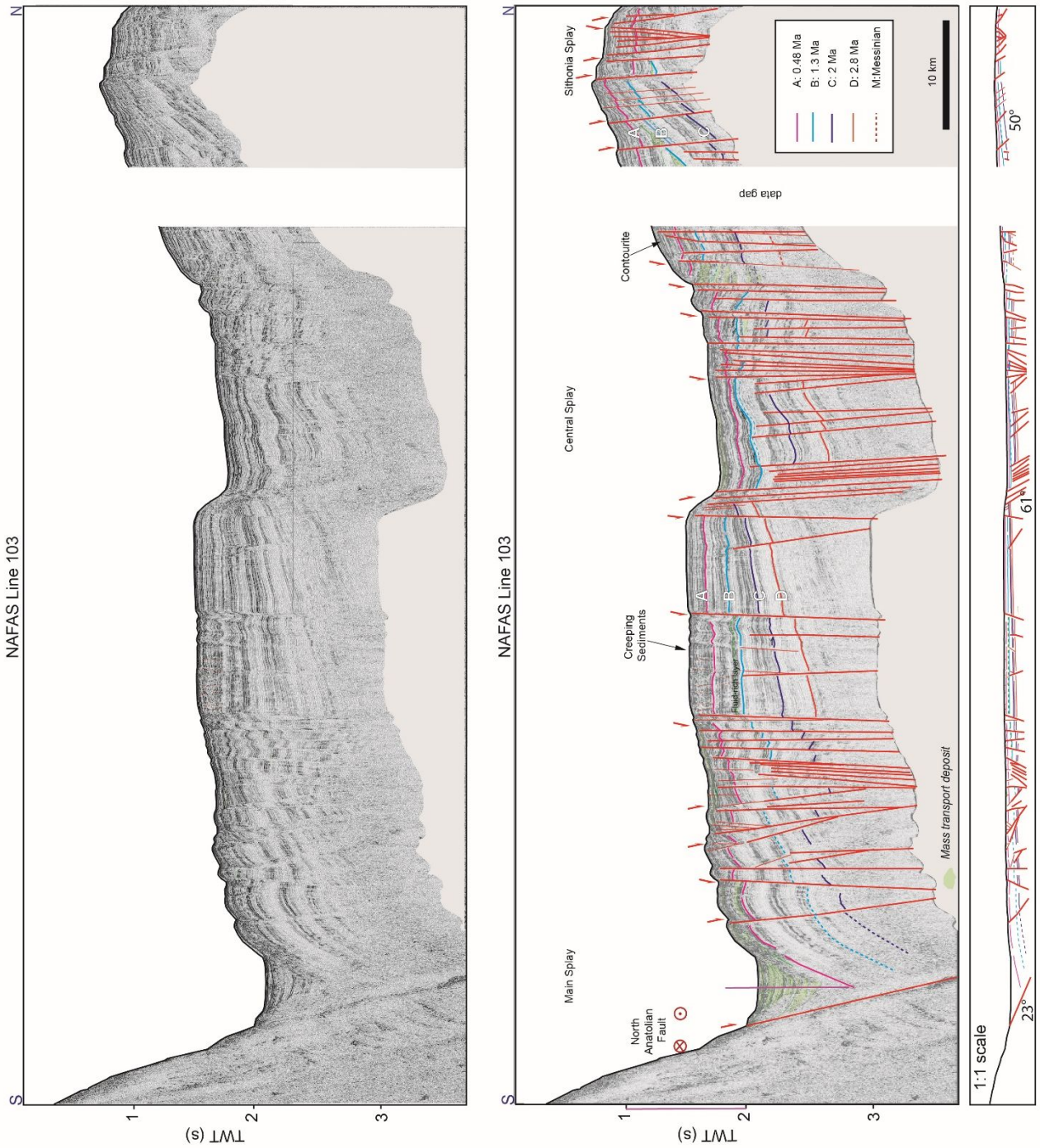
674 **Figure 10:** Seismic line 602 from the NAFAS cruise, crossing the main splay of the North Anatolian
 675 Fault, the central high and the Sithonia splay within the North Aegean Trough. See figure 3 for location.



676

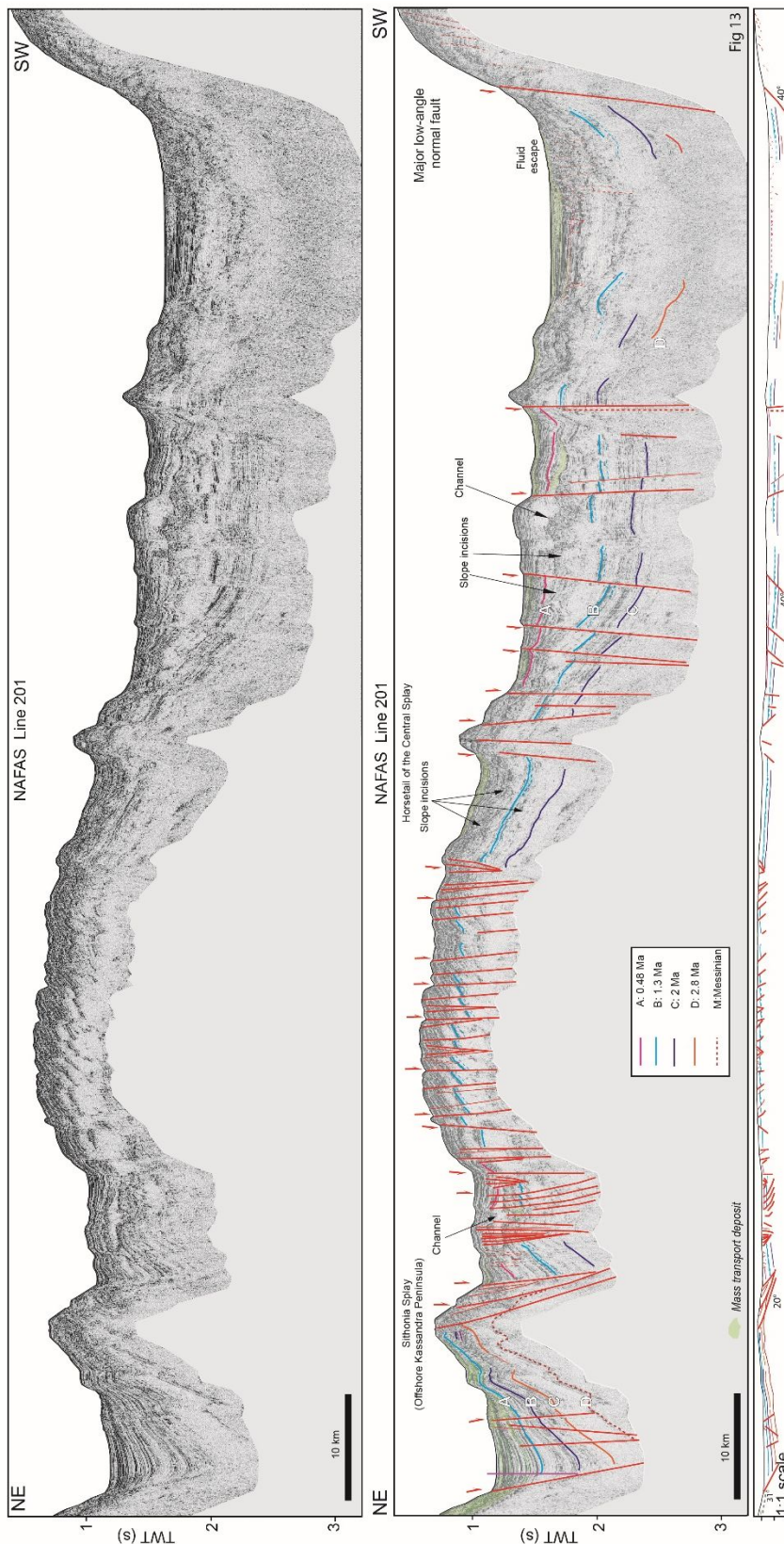
677 **Figure 11:** Seismic line 603 from the NAFAS cruise, crossing the main splay of the North Anatolian

678 Fault, the central high and the Sithonia splay within the North Aegean Trough. See figure 3 for location.

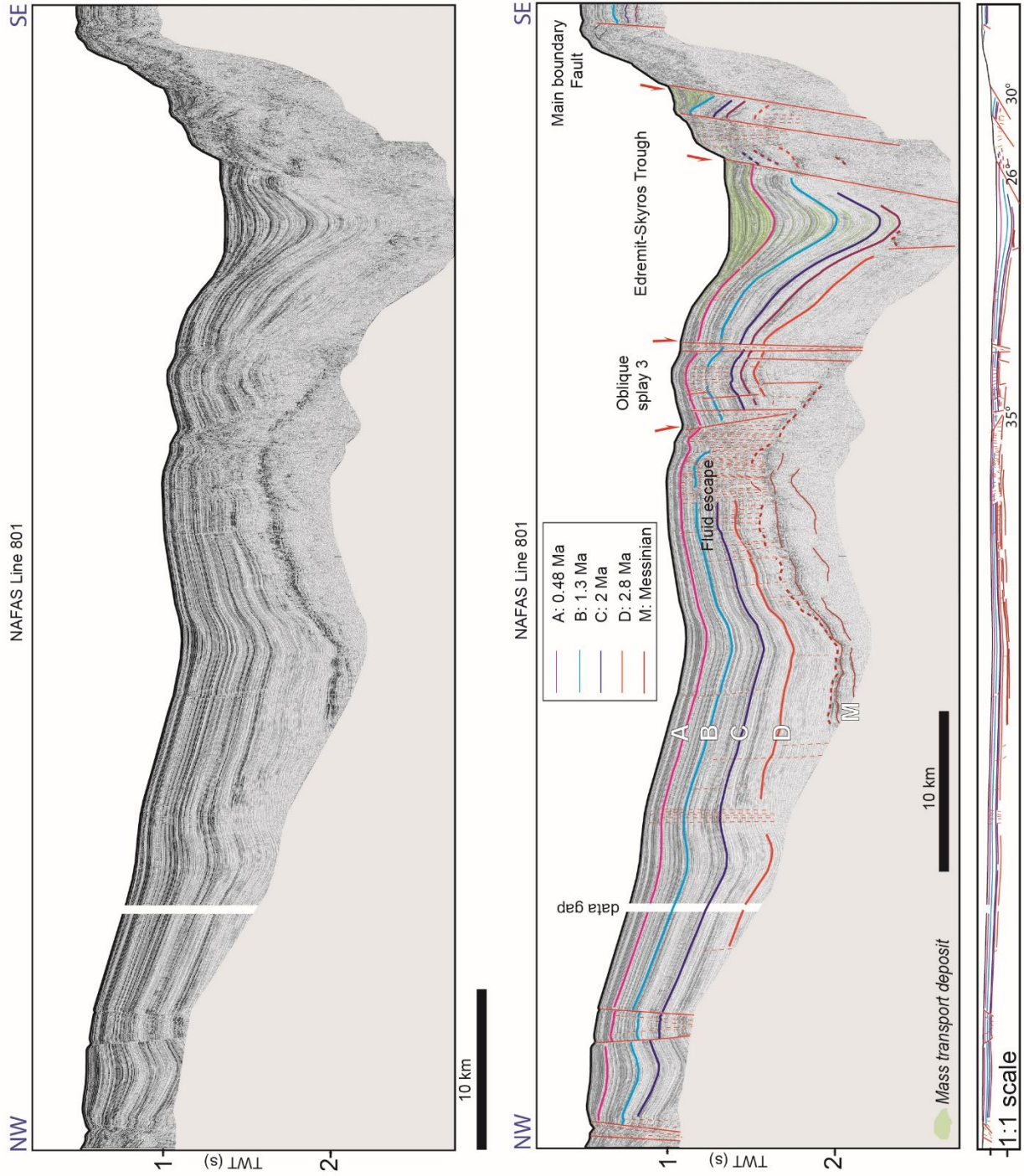


679

680 **Figure 12:** Seismic line 103 from the NAFAS cruise, crossing the Main splay of the North Anatolian
 681 Fault, the central splay and the western termination of the Sithonia Splay within the North Aegean
 682 Trough. See figure 3 for location



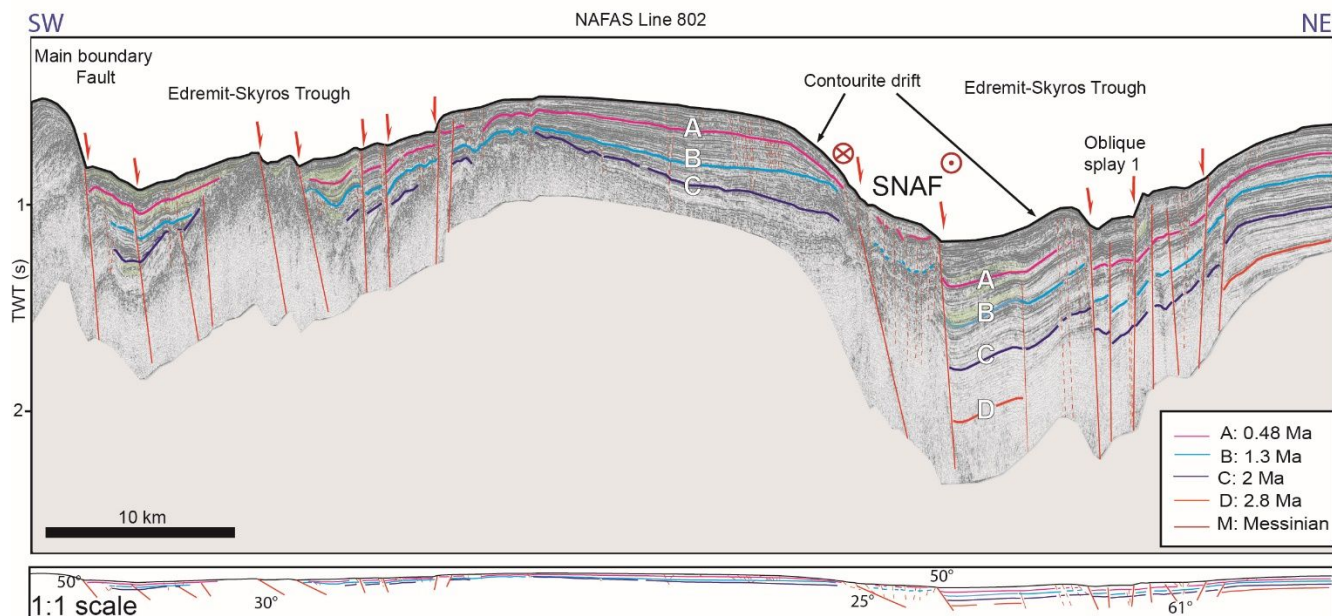
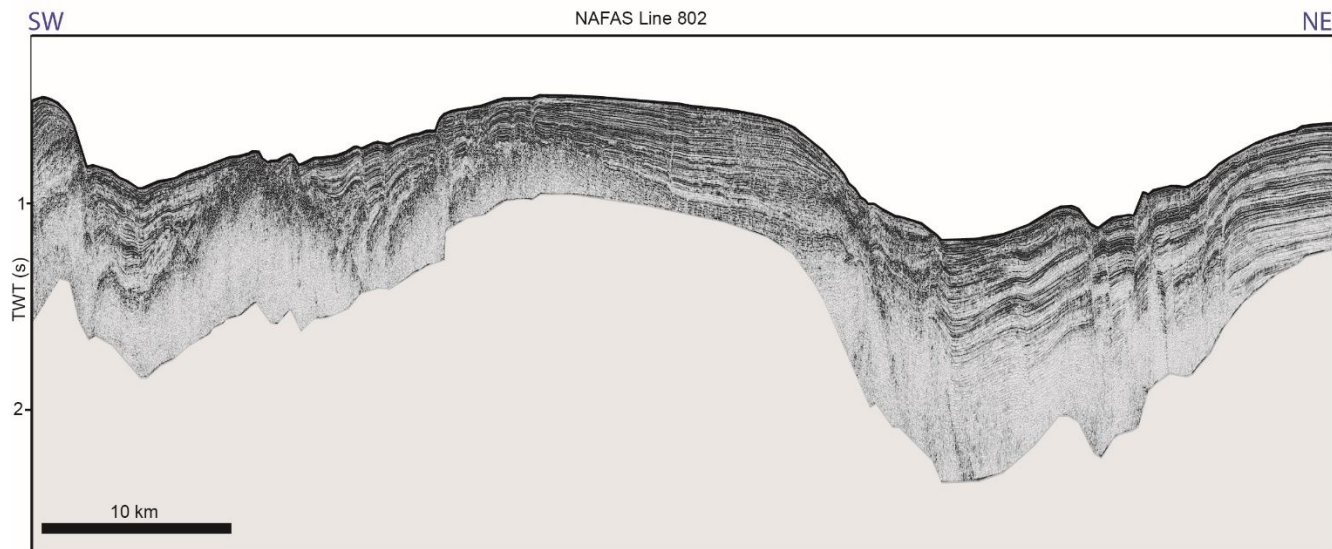
683
 684 **Figure 13:** Seismic line 201 from the NAFAS cruise, crossing the series of oblique splays dissecting
 685 the slope at the edge of the Gulf of Thermaïkos and a field of fluid escape features. See figure 3 for
 686 location.



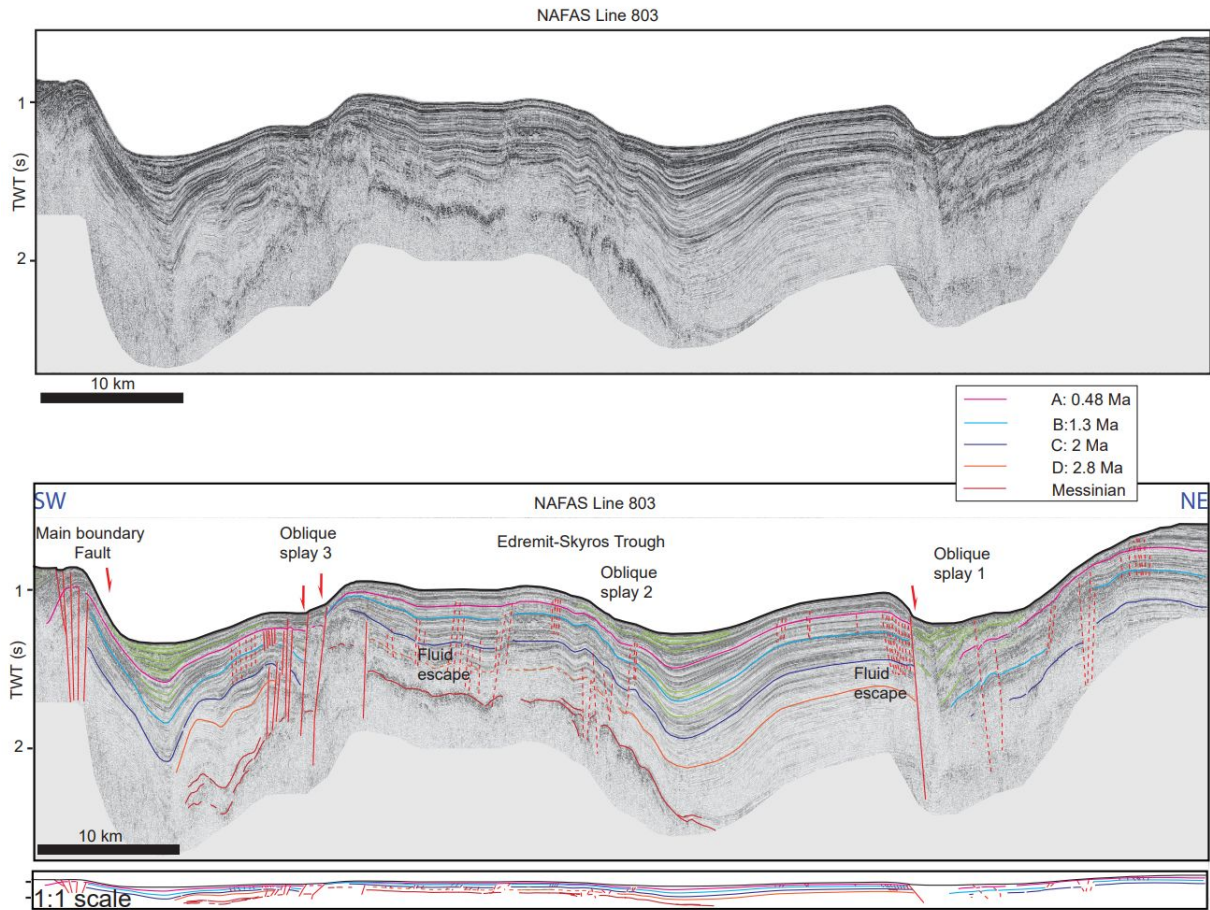
687

688 **Figure 14:** Seismic line 801 from the NAFAS cruise, crossing the Edremit-Skyros Trough. See figure

689 3 for location.



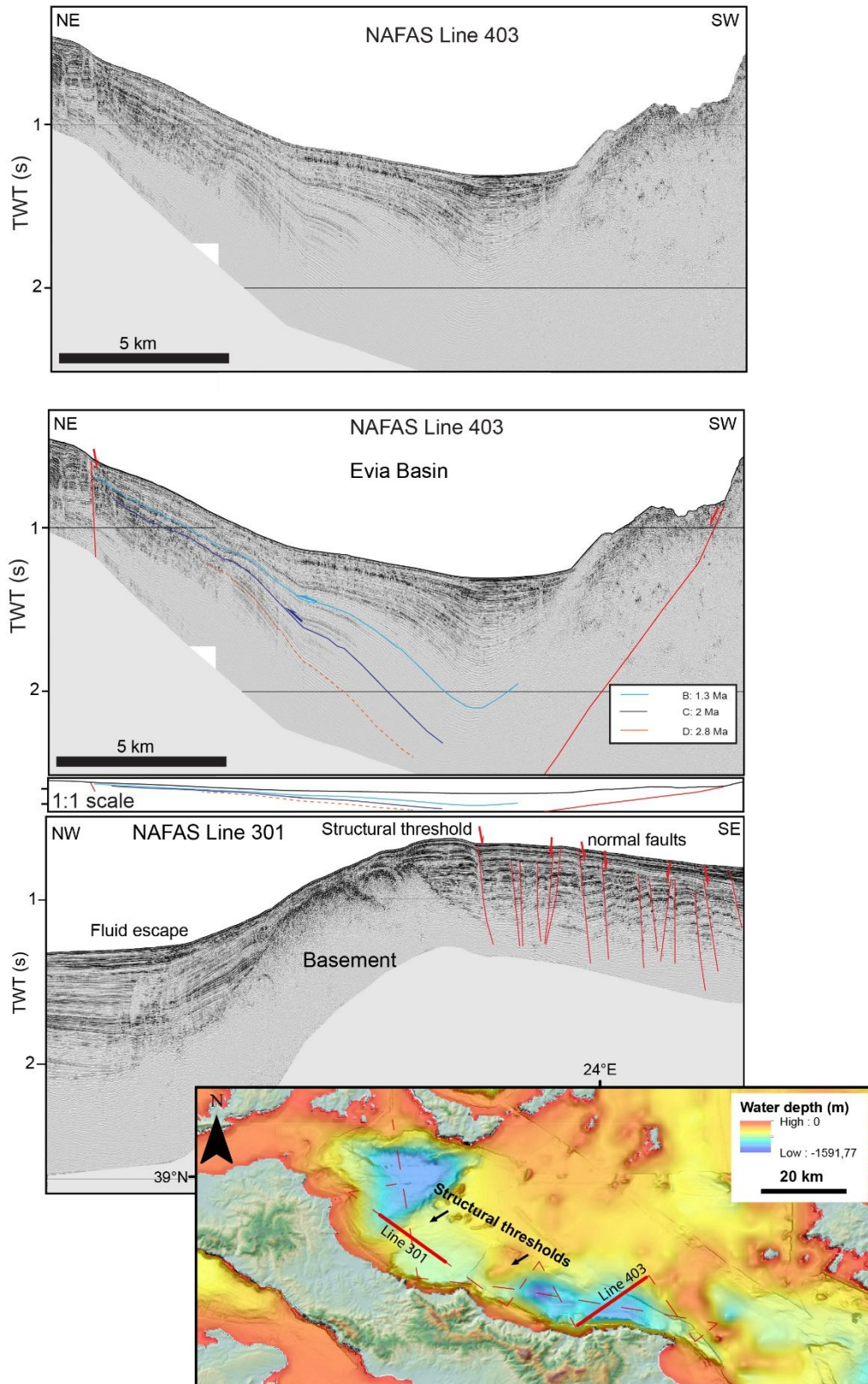
690
691 **Figure 15:** Seismic line 802 from the NAFAS cruise, crossing the Edremit-Skyros Trough. See figure
692 3 for location.



693

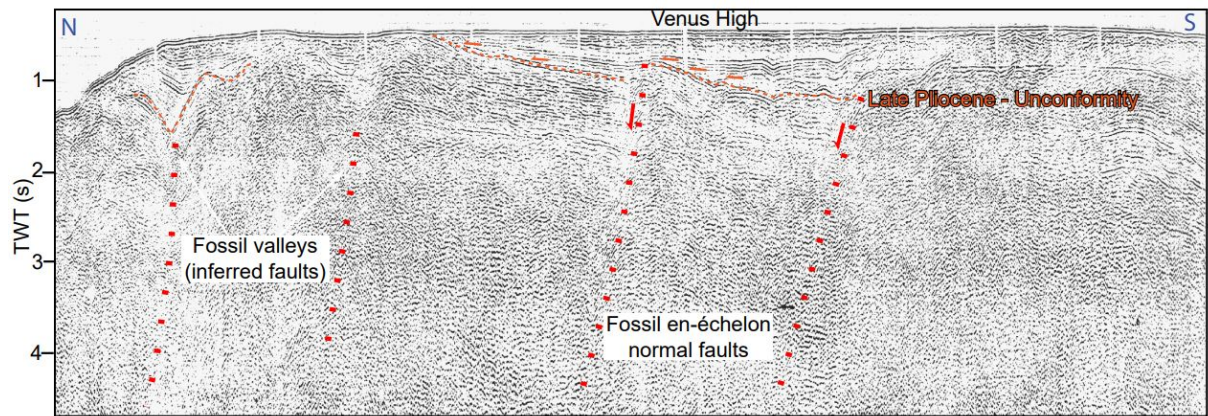
694 **Figure 16:** Seismic line 803 from the NAFAS cruise, crossing the Edremit-Skyros Trough. See figure
 695 3 for location.

695



696

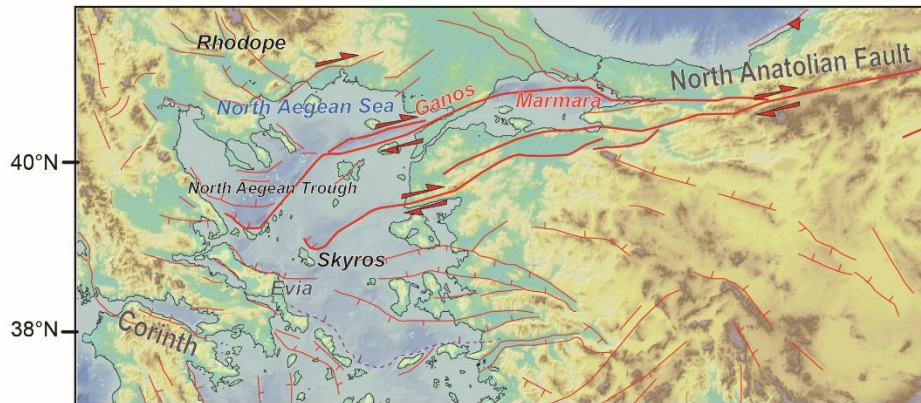
697 **Figure 17:** Seismic line 401 from the NAFAS cruise, crossing the main normal fault bounding the Evia
 698 Basin and seismic line 301 crossing one of the structural thresholds identified within the Evia basin. See
 699 inset and figure 3 for location.



700

701 **Figure 18:** Vintage seismic line, from Beniest et al. (2016), showing the Venus graben. See figure 3 for

702 location.

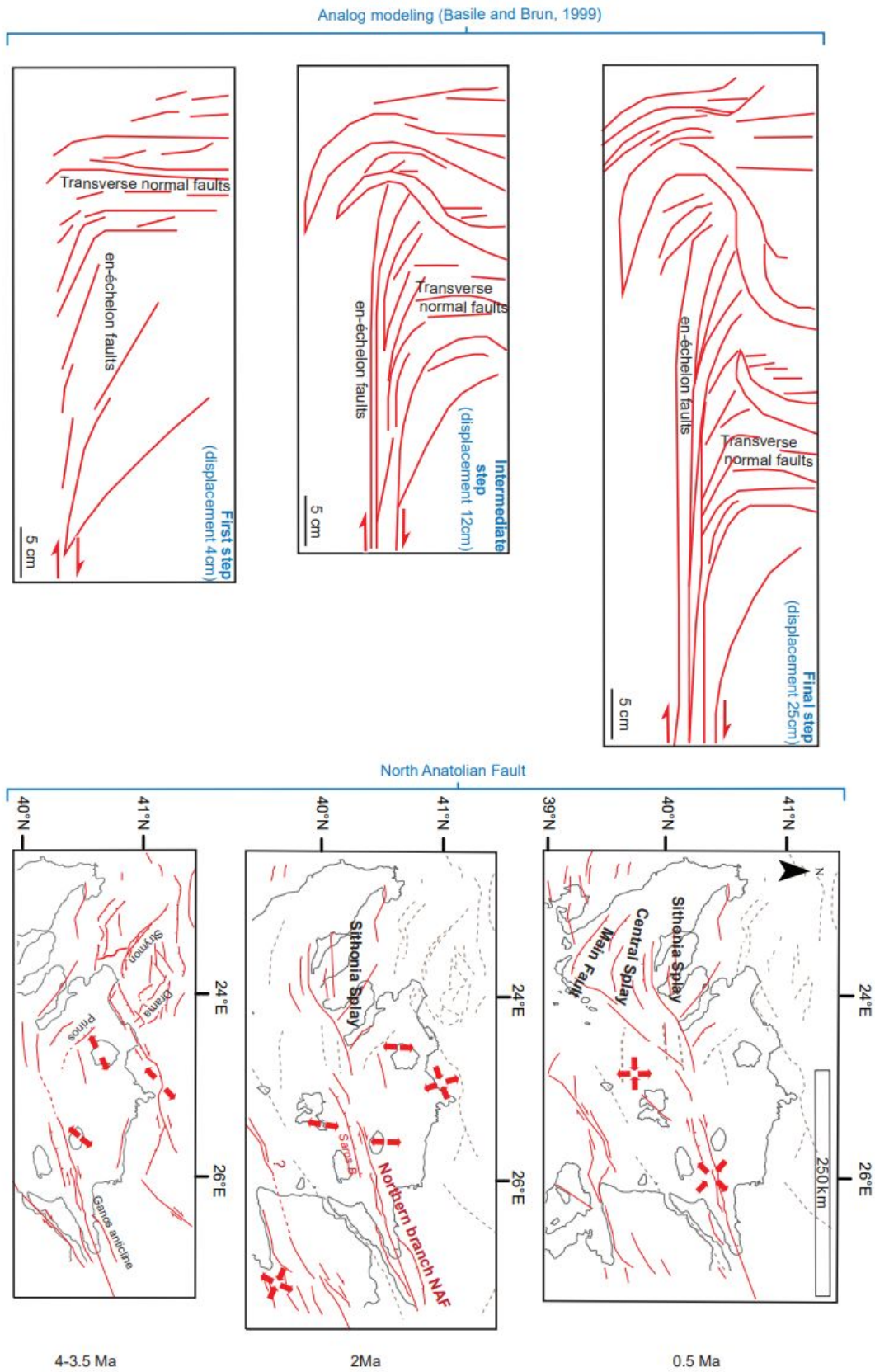


	Corinth	Rhodope & North Aegean Sea	Marmara & Ganos
Late Miocene		*Opening of Strymon, Orfanos, Mygdonia, and Drama Basins (Brun & Sokoutis, 2018)	*Diffuse strike-slip system (Thrace Basin) *First stage of the Southern branch of the NAF (Le Pichon et al., 2015)
Messinian Event			
Pliocene	*Distributed extension south of the Corinth rift -Early Pliocene (Collier & Dart, 1991)	*Opening of Prinos Basin (Proedrou & Papaconstantinou, 2004) *Deactivation of Venus and Athos Grabens at 2.8 Ma (this study)	*Ganos Fold (Armijo et al., 1999) *South Marmara Fault & Restraining bend Early Pliocene-3.5 Ma (Le Pichon et al., 2014)
Pleistocene	*Migration of deformation within the Corinth Rift & Distributed deformation Early Pleistocene (Nixon et al., 2016) *Migration of fault activity within the Corinth Rift between 0.6 -0.34 Ma *Strain localization since 0.34 Ma (Nixon et al., 2016)	*Sequential formation of the North Aegean Trough: *Sithonia Splay & Skyros Basin since 2-1.3 Ma (this study) *Central Splay of the North Aegean Trough since 1.3 Ma (this study) *Opening of the Evia Basin since 1.3 Ma (this study) * Main Splay of the NAF within the North Aegean Trough since 0.5 Ma (Ferentinos et al., 2018; this study) *Alonissos splay since 0.1-0.2Ma (Porkolab et al., 2023)	*Main Marmara Fault (emplacement between 0.5 & 2.5 Ma) (Grall et al., 2013; Le Pichon et al., 2015) *Reorganization of the Southern branch of the NAF at 0.5-1.3 Ma (Demoulin et al. 2013)

703

704 **Figure 19:** Summary of the main steps of structural evolution of the North Anatolian Fault and the Gulf

705 of Corinth in the North Aegean Domain.

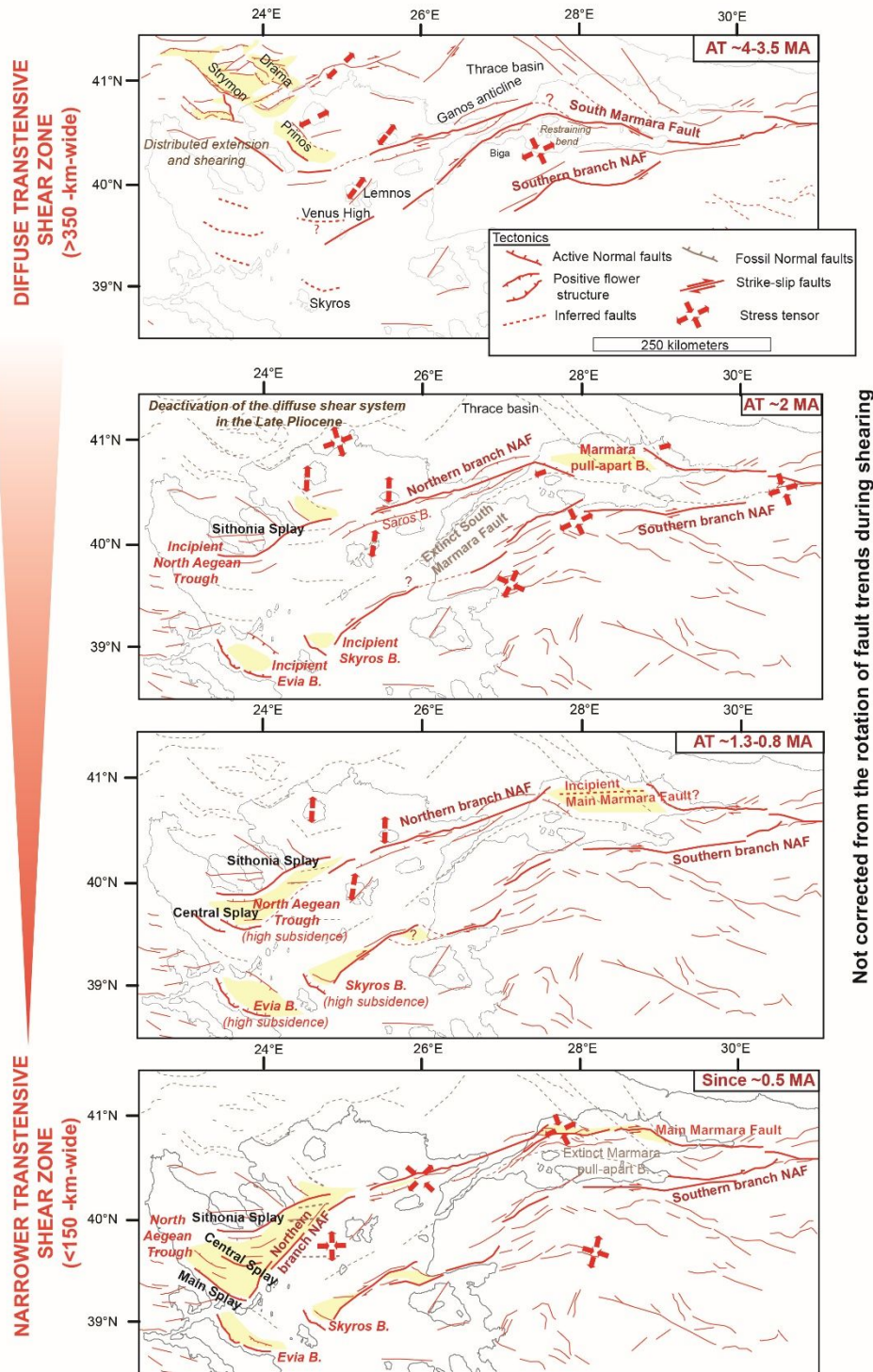


706

707 **Figure 20:** Analog (sandbox) models for the evolution of horsetail termination, from Basile and Brun

708 (1999), compared with the evolution of the North Aegean Trough horsetail (this study).

709



710

711 **Figure 21:** Structural evolution of the North Anatolian Fault in the North Aegean Domain, compiling
 712 field and offshore observations. This series of maps represents the present-day location of the faults that
 713 used to be active at 4-3.5 Ma, 2 Ma, 1.3-0.8 Ma, 0.5 Ma. The past shorelines are not reconstructed.
 714 Paleo-stress tensors from Sümer et al. (2018) and Lybéris (1984).

1
2
3 715 **References**
4

- 5 716 Anastasakis, G. & Piper, D.J.W., 2005. Late Neogene evolution of the western South Aegean volcanic
6
7 717 arc: sedimentary imprint of volcanicity around Milos, *Mar. Geol.*, **215**, 135-158.
- 8
9 718 Anastasakis, G., Piper, D.J.W., Dermitzakis, M.D., Karakitsios, V., 2006. Upper Cenozoic stratigraphy
10
11 719 and paleogeographic evolution of Myrtoon and adjacent basins, Aegean Sea, Greece, *Mar. Pet. Geol.*,
12
13 720 **23**, 353-369.
- 14
15 721 Anastasakis, G., Piper, D.J.W., 2013. The changing architecture of sea-level lowstand deposits across
16
17 722 the Mid-Pleistocene transition: South Evoikos Gulf, Greece, *Quaternary Science Reviews*, **73**, 103-114.
- 18
19 723 Armijo, R., Lyon-Caen, H., Papanastassiou, D., 1992. East-west extension and Holocene normal-fault
20
21 724 scarps in the Hellenic arc, *Geology*, **20**, 491-494.
- 22
23 725 Armijo, R., Meyer, B., King, G.C.P., Rigo, A., Papanastassiou, D., 1996. Quaternary evolution of the
24
25 726 Corinth Rift and its implications for the Late Cenozoic evolution of the Aegean, *Geophys. J. Int.*, **126**,
26
27 727 11-53.
- 28
29 728 Armijo, R., Meyer, B., Hubert, A., Barka, A., 1999. Westward propagation of the North Anatolian fault
30
31 729 into the northern Aegean: Timing and kinematics, *Geology*, **27**, 267-270.
- 32
33 730 Basile, C. & Brun, J.-P., 1999. Transtensional faulting patterns ranging from pull-apart basins to
34
35 731 transform continental margins: an experimental investigation. *J. Struct. Geol.*, **21**, 23-37.
- 36
37 732 Beniest, A., Brun, J.-P., Gorini, C., Crombez, V., Deschamps, R., Hamon, Y., Smit, J., 2016. Interaction
38
39 733 between trench retreat and anatolian escape as recorded by neogene basins in the northern Aegean Sea.
40
41 734 *Mar. Pet. Geol.*, **77**, 30-42.
- 42
43 735 Ben-Zion, Y. & Sammis, C.G., 2003. Characterization of fault zones. *Pure Applied Geophysics*, **160**,
44
45 736 677-715.
- 46
47 737 Brooks, M. & Ferentinos, G., 1980. Structure and evolution of the Sporadhes basin of the North Aegean
48
49 738 trough, northern Aegean Sea. *Tectonophysics*, **68**, 15-30.
- 50
51 739 Brun, J.-P., Faccenna, C., Gueydan, F., Sokoutis, D., Philippon, M., Kydonakis, K., Gorini, C., 2016.
52
53 740 The two-stage Aegean extension, from localized to distributed, a result of slab rollback acceleration.
54
55 741 *Canadian Journal of Earth Sciences*, **53**, 1142-1157.
- 56
57
58
59
60

- 1
2
3 742 Brun, J.-P. & Sokoutis, D., 2018. Core complex segmentation in North Aegean, a dynamic view.
4
5 743 *Tectonics*, **37**, doi: 10.1029/2017TC004939
6
7 744 Brun, J.-P. & Faccenna, C., 2008. Exhumation of high-pressure rocks driven by slab rollback. *Earth*
8
9 745 *Planet. Sci. Lett.*, **272**, 1-7.
10
11 746 Bulut, F., Özener, H., Dogru, A., Aktug, B., Yaltrak, C., 2018. Structural setting along the Western
12
13 747 North Anatolian Fault and its influence on the 2014 North Aegean Earthquake (Mw 6.9).
14
15 748 *Tectonophysics*, **745**, 382–394, <https://doi.org/10.1016/j.tecto.2018.07.006>, 2018.
16
17 749 Calvo, J.P., Triantaphyllou, M.V., Regueiro, M., Stamatakis, M.G., 2012. Alternating diatomaceous and
18
19 750 volcanoclastic deposits in Milos Island, Greece. A contribution to the upper Pliocene-lower Pleistocene
20
21 751 stratigraphy of the Aegean Sea. *Palaeogeography, Palaeoclimatology, Palaeoecology*, **321-322**, 24-40.
22
23 752 Caroir, F., Chanier, F., Gaullier, V., Sakellariou, D., Bailleul, J., Maillard, A., Paquet, F., Watemez, L.,
24
25 753 Averbuch, O., Graveleau, F., Ferrière, J., 2023. Plio-Quaternary deformations within the North Evia
26
27 754 domain (Greece) in the western prolongation of the North Anatolian Fault: insights from very high-
28
29 755 resolution seismic data (WATER surveys). Available at SSRN: <https://ssrn.com/abstract=4341779> or
30
31 756 <http://dx.doi.org/10.2139/ssrn.4341779>
32
33 757 Carton, H., Singh, S.C., Hirn, A., Bazin, S., de Voogd, B., Vigner, A., Ricolleau, A., Cetin, S., Karakoç,
34
35 758 F., Sevilgen, V., 2007. Seismic imaging of the three-dimensional architecture of the Cinarcik basin along
36
37 759 the North Anatolian Fault. *J. Geophys. Res.*, **112**, B06101, doi:10.1029/2006JB004548
38
39 760 Chamot-Rooke, N., et al., 2005. DOTMED: A Synthesis of Deep Marine Data in the Eastern
40
41 761 Mediterranean, *Mem. Soc. Geol. Fr.*, **177**, 64 pp.
42
43 762 Collier, R. E. L. & Dart, C.J., 1991. Neogene to Quaternary rifting, sedimentation and uplift in the
44
45 763 Corinth Basin, Greece. *J. Geol. Soc. London*, **148**(6), 1049– 1065, doi:10.1144/gsjgs.148.6.1049
46
47 764 de Gelder, G., Fernández-Blanco, D., Öğretmen, N., Liakopoulos, S., Papanastassiou, D., Faranda, C.,
48
49 765 Armijo, R., Lacassin, R., 2022. Quaternary E-W extension uplifts Kythira Island and segments the
50
51 766 Hellenic Arc, *Tectonics*, <https://doi.org/10.1029/2022TC007231>
52
53 767 Demoulin, A., Altin, T.B., Beckers, A., 2013. Morphometric age estimate of the last phase of accelerated
54
55 768 uplift in the Kazdag area (Biga Peninsula, NW Turkey). *Tectonophysics*, **608**, 180-1393,
56
57 769 <https://doi.org/10.1016/j.tecto.2013.06.004>
58
59
60

- 1
2
3 770 Dietrich, V.J., Mercolli, I., Oberhänsli, R., 1988. Dazite, High-Alumina Basalte und Andesite als
4
5 771 Produkte amphiboldominierter Differentiation (Aegina und Methan, Agaischer Inselbogen).
6
7 772 *Schweizische Mineralogische und Petrographische Mitteilungen*, **68**, 21–39.
8
9 773 Dooley, T. & Schreurs, G., 2012. Analogue modelling of intraplate strike-slip tectonics: a review and
10
11 774 new experimental results. *Tectonophysics*, **574-575**, 1-71.
12
13 775 Endrun, B., Lebedev, S., Meier, T., Tirel, C., Friederich, W., 2011. Complex layered deformation within
14
15 776 the Aegean crust and mantle revealed by seismic anisotropy. *Nature Geosci.*, **4**, 203-207
16
17 777 England, P., Houseman, G., Nocquet, J.-M., 2016. Constraints from GPS measurements on the dynamics
18
19 778 of deformation in Anatolia and the Aegean. *J. Geophys. Res. Solid Earth*, **121**, 8888–8916,
20
21 779 doi:10.1002/2016JB013382.
22
23 780 Faccenna, C., Bellier, O., Martinod, J., Piromallo, C., Regard, V., 2006. Slab detachment beneath eastern
24
25 781 Anatolia: A possible cause for the formation of the North Anatolian fault. *Earth Planet. Sci. Lett.*, **242**,
26
27 782 85–97.
28
29 783 Faugères, J.C., Gonthier, E., Mulder, T., Kenyon, N., Cirac, P., Griboulard, R., Berné, S., Lesuavé, R.,
30
31 784 2002. Multiprocess generated sediment waves on the Landes Plateau (Bay of Biscay, North Atlantic).
32
33 785 *Mar. Geol.*, **182**, 279-302.
34
35 786 Ferentinos, G., Brooks, M., Collins, M., 1981. Gravity-induced deformation on the north flank and floor
36
37 787 of the Sporadhes Basin of the North Aegean Sea Trough. *Mar. Geol.*, **44**, 289–302.
38
39 788 Ferentinos, G., Georgiou, N., Christodoulou, D., Geraga, M., Papatheodorou, G., 2018. Propagation and
40
41 789 termination of a strike slip fault in an extensional domain: The westward growth of the North Anatolian
42
43 790 Fault into the Aegean Sea. *Tectonophysics*, **745**, 183–195, <https://doi.org/10.1016/j.tecto.2018.08.003>,
44
45 791 2018.
46
47 792 Fernàndez-Blanco, D., de Gelder, G., Lacassin, R., Armijo, R., 2019. A new crustal fault formed the
48
49 793 modern Corinth Rift. *Earth Sci. Rev.*, **199**, 102919
50
51 794 Flerit, F., Armijo, R., King, G., Meyer, B., 2004. The mechanical interaction between the propagating
52
53 795 North Anatolian Fault and the back-arc extension in the Aegean. *Earth Planet. Sci. Lett.*, **224**, 347-362.
54
55 796 Floyd, M. A., et al., 2010. A new velocity field for Greece: Implications for the kinematics and dynamics
56
57 797 of the Aegean, *J. Geophys. Res.*, **115**, B10403, doi:10.1029/2009JB007040

- 1
2
3 798 Ford, M., Rohais, S., Williams, E. A., Bourlange, S., Jousselin, D., Backert, N., Malartre, F., 2013.
4
5 799 Tectono-sedimentary evolution of the western Corinth rift (Central Greece). *Basin Res.*, **25**, 3-25, doi :
6
7 800 10.1111/j.1365-2117.2012.00550.x
8
9 801 Fournier, M., Chamot-Rooke, N., Rodriguez, M., Huchon, P., Petit, C., Beslier, M-O., 2011. Owen
10
11 802 Fracture Zone: the Arabia-India plate boundary unveiled. *Earth Planet. Sci. Lett.*, **302**, 247-252, doi:
12
13 803 10.1016/j.epsl.2010.12.027
14
15 804 Fytikas, M., Giuliani, O., Innocenti, F., Marinelli, G., Mazzuoli, R., 1976. Geochronological data on
16
17 805 recent magmatism of the Aegean Sea. *Tectonophysics*, **31**, 29-4.
18
19 806 Fytikas, M., Innocenti, F., Kolios, N., Manetti, P., Mazzuoli, R., Poli, G., Rita, F., Villari, L., 1986.
20
21 807 Volcanology and petrology of volcanic products from the island of Milos and neighbouring islets.
22
23 808 *Journal of volcanology and geothermal research*, **28**, 297-317.
24
25 809 Garfunkel, Z. & Ben-Avraham, Z., 1996. The structure of the Dead Sea basin. *Tectonophysics*, **266**,
26
27 810 155-176, doi:10.1016/S0040-1951(96)00188-6
28
29 811 Grall, C., Henry, P., Tezcan, D., Géli, L., de Lepinay, B-M., Rudkiewicz, J-L., Zitter, T., Harmegnies,
30
31 812 F., 2012. Heat flow in the Sea of Marmara Central Basin: Possible implications for the tectonic evolution
32
33 813 of the North Anatolian Fault. *Geology*, **40**, 3-6, <https://doi.org/10.1130/g32192.1>.
34
35 814 Grall, C., Henry, P., Thomas, Y., Westbrook, G., Çagatay, M., Marsset, B., Saritas, H., Çifçi, G., Geli,
36
37 815 L., 2013. Slip rate estimation along the western segment of the Main Marmara Fault over the last 405–
38
39 816 490 ka by correlating mass transport deposits. *Tectonics*, **32**, 1587–1601
40
41 817 Gürer, Ö., Sangu, E., Özburan, M., Gürbüz, A., Gürer, A., Simir, H., 2016. Plio-Quaternary kinematic
42
43 818 development and paleostress pattern of the Edremit Basin, Western Turkey. *Tectonophysics*, **679**, 199-
44
45 819 210. <http://dx.doi.org/10.1016/j.tecto.2016.05.007>
46
47 820 Handy, M.R., Schmid, S.M., Bousquet, R., Kissling, E., Bernoulli, D., 2010. Reconciling plate-tectonic
48
49 821 reconstructions of Alpine Tethys with the geological-geophysical record of spreading and subduction in
50
51 822 the Alps. *Earth Sci. Rev.*, **102**, 121-158. Doi:10.1016/j.earscirev.2010.06.002
52
53 823 Hébert, H., Schindele, F., Altinok, Y., Alpar, B., Gazioglu, C., 2005. Tsunami hazard in the Marmara
54
55 824 Sea (Turkey): a numerical approach to discuss active faulting and impact on the Istanbul coastal areas.
56
57 825 *Mar. Geol.*, **215**, 23–43.

- 1
2
3 826 Hsu, K. J., Montadert, L., Bernouilli, D., Bizon, G., Cita, M., Ericson, A., Fabricius, F., Garrison, R.E.,
4
5 827 Kidd, R.B., Melieres, F., Müller, C., Wright, R.C., 1978. Site 378, Cretan Basin. Init Rep. DSDP, **42**,
6
7 828 321-357.
8
9 829 Hubert-Ferrari, A., Barka, A., Jacques, E., Nalbant, S. S., Meyer, B., Armijo, R., Tapponnier, P., King,
10
11 830 G. C. P., 2000. Seismic hazard in the Marmara Sea region following the 17 August 1999 Izmit
12
13 831 earthquake. *Nature*, **404**, 269-273.
14
15 832 Hubert Ferrari, A., King, G., Van der Woerd, J., Villa, I., Altunel, E., Armijo, R., 2010. Long-term
16
17 833 evolution of the North Anatolian Fault: new constraints from its eastern termination. From: VAN
18
19 834 HINSBERGEN, D. J. J., EDWARDS, M. A. & GOVERS, R. (eds) Collision and Collapse at the Africa–
20
21 835 Arabia–Eurasia Subduction Zone. *Geol. Soc. London, Spec. Pub.*, **311**, 133–154. DOI: 10.1144/SP311.5
22
23 836 Islamoglu, Y., Harzhauser, M., Gross, M., Jimenez-Moreno, G., Coric, S., Kroh, A., Rögl, F., van der
24
25 837 Made, J., 2008. From Tethys to eastern Paratethys: Oligocene depositional environments, paleoecology
26
27 838 and paleobiogeography of the Thrace Basin (NW Turkey). *Int. J. Earth Sci.*, **18**, 183-200.
28
29 839 Isler, E., Aksu, A., Yalırak, C., Hiscott, R., 2008. Seismic stratigraphy and Quaternary sedimentary
30
31 840 history of the northeast Aegean Sea. *Mar. Geol.*, **254**, 1–17.
32
33 841 Janin, A., Rodriguez, M., Sakellariou, D., Lykousis, V., Gorini, C., 2019. Tsunamigenic potential of a
34
35 842 Holocene submarine landslide along the North Anatolian Fault (northern Aegean Sea, off Thasos
36
37 843 island): insights from numerical modelling. *Nat. Haz. Earth Syst. Sci.*, **19**, 121–136,
38
39 844 <https://doi.org/10.5194/nhess-19-121-2019>.
40
41 845 Jolivet, L., Faccenna, C., 2000. Mediterranean extension and the Africa-Eurasia collision. *Tectonics*, **19**,
42
43 846 1095–1106.
44
45 847 Jolivet, L. & Brun, J.-P., 2010. Cenozoic geodynamic evolution of the Aegean. *Int. J. Earth Sci.*, **99**,
46
47 848 109-138, doi: 10.1007/s00531-008-0366-4
48
49 849 Jolivet, L., Lecomte, E., Huet, B., Denèle, Y., Lacombe, O., Labrousse, L., Le Pourhiet, L., Mehl, C.,
50
51 850 2010. The North Cycladic Detachment System. *Earth Planet. Sci. Lett.*, **289**, 87-104.
52
53 851 Jolivet, L., Faccenna, C., Huet, B., Labrousse, L., Le Pourhiet, L., Lacombe, O., Lecomte, E., Burov,
54
55 852 E., Denele, Y., Brun, J.-P., Philippon, M., Paul, A., Salaün, G., Karabulut, H., Piromallo, C., Monié, P.,
56
57
58
59
60

- 1
2
3 853 Gueydan, F., Okay, A. I., Oberhänsli, R., Pourteau, A., Augier, R., Gadenne, L., Driussi, O., 2013.
4
5 854 Aegean tectonics: Strain localisation, slab tearing and trench retreat. *Tectonophysics*, **597**, 1–33.
6
7 855 Jolivet, L., Menant, A., Sternai, P., Rabillard, A., Arbaret, L., Augier, R., Laurent, V., Beaudoin, A.,
8
9 856 Grasemann, B., Huet, B., Labrousse, L., Le Pourhiet, L., 2015. The geological signature of a slab tear
10
11 857 below the Aegean. *Tectonophysics*, **659**, 166–182.
12
13 858 Jolivet, L., Menant, A., Roche, V., Le Pourhiet, L., Maillard, A., Augier, R., Do Couto, D., Gorini, C.,
14
15 859 Thinon, I., Canva, I., 2021. Transfer zones in Mediterranean back-arc regions and tear faults. *Bull. Soc.*
16
17 860 *Géol. France*, **192** (1), 11, <https://doi.org/10.1051/bsgf/2021006>
18
19 861 Jolivet, R., Lasserre, C., Doin, M.-P., Guillaso, S., Peltzer, G., Dailu, R., Sun, J., Shen, Z.-K., Xu, X.,
20
21 862 2012. Shallow creep on the Haiyuan Fault (Gansu, China) revealed by SAR interferometry. *J. Geophys.*
22
23 863 *Res. Solid Earth*, **117**, <https://doi.org/10.1029/2011JB008732>
24
25 864 Karakas, C., Armijo, R., Lacassin, R., Suc, J.-P., Melinte-Drobinescu, M.C., 2018. Crustal strain in the
26
27 865 Marmara pull-apart region associated with the propagation process of the North Anatolian Fault.
28
29 866 *Tectonics*, **7**, 1507-1523. <https://doi.org/10.1029/2017TC004636>
30
31 867 Karakitsios, V., Corné, J.-J., Tsourou, T., Moissette, P., Kontakiotis, G., Agiadi, K., Manoutsoglou, E.,
32
33 868 Triantaphyllou, M., Koskeridou, E., Drinia, H., Roussos, D., 2017. Messinian salinity crisis record under
34
35 869 strong freshwater input in marginal, intermediate, and deep environments: the case of the North Aegean.
36
37 870 *Palaogeography, Palaeoclimatology, Palaeoecology*, **485**, 316-335
38
39 871 Kiratzi, A. & Louvari, E., 2003. Focal mechanisms of shallow earthquakes in the Aegean Sea and the
40
41 872 surrounding lands determined by waveform modelling: a new database. *J. of Geodyn.* **36**, 251-274.
42
43 873 Konstantinou, K.I., Mouslopoulou, V., Liang, W.-T., Heidbach, O., Oncken, O., Suppe, J., 2017. Present-
44
45 874 day crustal stress field in Greece inferred from regional-scale damped inversion of earthquake focal
46
47 875 mechanisms. *J. Geophys. Res. Solid Earth*, **122**, 506-523, doi:10.1022/2016JB013272
48
49 876 Koukouvelas, I.K. & Aydin, A., 2002. Fault structure and related basins of the North Aegean Sea and
50
51 877 its surroundings. *Tectonics*, **21**, <https://doi.org/10.1029/2001TC901037>
52
53 878 Kourouklas, C., Tsaklidis, G., Papadimitriou, E., Karakostas, V., 2022. Analyzing the Correlations and
54
55 879 the Statistical Distribution of Moderate to Large Earthquakes Interevent Times in Greece. *Appl. Sci.*, **12**,
56
57 880 7041. <https://doi.org/10.3390/app12147041>
58
59
60

- 1
2
3 881 Kreemer, C., Holt, W.E., Haines, A.J., 2003. An integrated global model of present-day plate motions
4
5 882 and plate boundary deformation. *Geophys. J. Int.*, **154**, 8-34, <https://doi.org/10.1046/j.1365->
6
7 883 246X.2003.01917.x
8
9 884 Kreemer, C. & Chamot-Rooke, N., 2004. Contemporary kinematics of the Southern Aegean and the
10
11 885 Mediterranean Ridge. *Geophys. J. Int.*, **157**, 1377-1392, doi:10.1111/j.1365-246X.2004-02270.x
12
13 886 Krijgsman, W., et al., 2022. Mediterranean-Black Sea gateway exchange: scientific drilling workshop
14
15 887 on the BlackGate project. *Sci. Dril.*, **31**, 93-110, <https://doi.org/10.5194/sd-31-93-2022>
16
17 888 Lafosse, M., d'Acremont, E., Rabaute, A., Estrada, F., Jollivet-Castelot, M., Vazquez, J.T., Galindo-
18
19 889 Zaldivar, J., Ercilla, G., Alonso, B., Smit, J., Ammar, A., Gorini, C., 2020. Plio-Quaternary tectonic
20
21 890 evolution of the southern margin of the Alboran Basin (Western Mediterranean). *Solid Earth*, **11**, 741–
22
23 891 765, <https://doi.org/10.5194/se-11-741-2020>
24
25 892 Laigle, M., Hirn, A., Sachpazi, M., Roussos, N., 2000. North Aegean crustal deformation: an active
26
27 893 fault imaged to 10 km depth by reflection seismic data. *Geology*, **28**, 71–74.
28
29 894 Lefevre, M., Souloumiac, P., Cubas, N., Klinger, Y., 2020. Experimental evidence for crustal control
30
31 895 over seismic fault segmentation. *Geology*, **48**, 844-848.
32
33 896 Le Pichon, X. & Kreemer, C., 2010. The Miocene-to-present kinematic evolution of the eastern
34
35 897 Mediterranean and Middle East and its implications for dynamics. *Annual Review Earth Planetary*
36
37 898 *Science*, **38**, 323–351.
38
39 899 Le Pichon, X., Sengör, A.M.C., Demirbag, E., Rangin, C., Imren, C., Armijo, R., Görür, N., Çagatay,
40
41 900 N., De Lepinay, B. M., Meyer, B., Saatçılar, R., Tok, B., 2001. The active main Marmara fault. *Earth*
42
43 901 *Planet. Sci. Lett.*, **192**, 595–616.
44
45 902 Le Pichon, X., Chamot-Rooke, N., Rangin, C., 2003. The North Anatolian fault in the Sea of Marmara.
46
47 903 *J. Geophys. Res.*, **108**, 2179, doi:10.1029/2002JB001862
48
49 904 Le Pichon, X., Imren, C., Rangin, C., Sengör, A.M.C., Siyako, M., 2014. The South Marmara Fault. *Int.*
50
51 905 *J. Earth Sci.*, **103**, 219–231.
52
53 906 Le Pichon, X., Sengör, A.M.C., Kende, J., Imren, C., Henry, P., Grall, C., Karabulut, H., 2015.
54
55 907 Propagation of a strike-slip plate boundary within an extensional environment: the westward
56
57 908 propagation of the North Anatolian Fault. *Canadian Journal Earth Sciences*, **53**, 1416–1439.
58
59
60

- 1
2
3 909 Le Pourhiet, L., Huet, B., May, D.A., Labrousse, L., Jolivet, L., 2012. Kinematic interpretation of the
4
5 910 3D shapes of metamorphic core complexes. *Geochem. Geophys. Geosyst.*, **13**,
6
7 911 <https://doi.org/10.1029/2012GC004271>
8
9 912 Le Pourhiet, L., Huet, B., Traoré, N., 2014. Links between long-term and short-term rheology of the
10
11 913 lithosphere: insights from strike-slip fault modelling. *Tectonophysics*, **631**, 146-159
12
13 914 Lyberis, N., 1984. Tectonic evolution of the North Aegean trough. *Geol. Soc. London Spec. Pub.*, **17**,
14
15 915 709-725, <https://doi.org/10.1144/GSL.SP.1984.017.01.57>
16
17 916 Lykousis, V., Roussakis, G., Alexandri, M., Pavlakis, P., Papoulia, I., 2002. Sliding and regional slope
18
19 917 stability in active margins: North Aegean Trough (Mediterranean). *Mar. Geol.*, **186**, 281–298.
20
21 918 Lykousis, V., 2009. Sea-level changes and shelf break prograding sequences during the last 400 ka in
22
23 919 the Aegean margins: subsidence rates and palaeogeographic implications. *Continental Shelf Research*,
24
25 920 **29**, 2037-2044.
26
27 921 Mann, P., 2007. Global catalogue, classification and tectonic origins of restraining- and releasing bends
28
29 922 on active and ancient strike-slip fault systems. *Geol. Soc. London Spec. Pub.*, **290**, 13-142.
30
31 923 Mascle, J. & Martin, L., 1990. Shallow structure and recent evolution of the Aegean Sea: A synthesis
32
33 924 based on continuous reflection profiles. *Mar. Geol.*, **94**, 271-299.
34
35 925 McNeill, L. C., Mille, A., Minshull, T. A., Bull, J. M., Kenyon, N.H., 2004. Extension of the North
36
37 926 Anatolian Fault into the North Aegean Trough: Evidence for transtension, strain partitioning, and
38
39 927 analogues for Sea of Marmara basin models. *Tectonics*, **23**, TC2016, doi:10.1029/2002TC001490
40
41 928 Mouslopoulou, V., Nicol, A., Little, T.A., Walsh, J.J., 2007a. Terminations of large strike-slip faults: an
42
43 929 alternative model from New Zealand. In: Cunningham, W. D. & Mann, P. (eds), *Tectonics of Strike-*
44
45 930 *Slip Restraining and Releasing Bends*. Geological Society of London, Special Publication 290, 387–
46
47 931 415, <http://sp.lyellcollection.org/content/290/1/387.short>.
48
49 932 Mouslopoulou, V., Nicol, A., Little, T.A., Walsh, J.J., 2007b. Displacement transfer between
50
51 933 intersecting strike-slip and extensional fault systems. *Journal of Structural Geology* **29**, 100-116,
52
53 934 <https://doi.org/10.1016/j.jsg.2006.08.002>.
54
55 935 Müller, M.D., Geiger, A., Kahle, H.-G., Veis, G., Billiris, H., Paradissis, D., Felekis, S., 2013. Velocity
56
57
58
59
60

- 1
2
3 936 and deformation fields in the North Aegean domain, Greece, and implications for fault kinematics,
4
5 937 derived from GPS data 1993-2009. *Tectonophysics*, **597-598**, 34-49.
6
7 938 Melinte-Drobinescou, M.C., Suc, J., Clauzon, G., Popescu, S.-M., Armijo, R., Meyer, B., Biltekin, D.,
8
9 939 Cagatay, N., Ucar, G., Jouanne, G., Fauquette, S., Cakir, Z., 2009. The messinian salinity crisis in
10
11 940 the dardanelles region: chronostratigraphic constraints. *Palaeogeography Palaeoclimatology*
12
13 941 *Palaeoecology*, **278**, 24-39, <http://dx.doi.org/10.1016/j.palaeo.2009.04.009>
14
15 942 Nixon, C. W., et al., 2016. Rapid spatiotemporal variations in rift structure during development of the
16
17 943 Corinth Rift, central Greece. *Tectonics*, **35**, 1225–1248, doi:10.1002/2015TC004026
18
19 944 Okay, A.I. & Tüysüz, O., 1999. Tethyan sutures of northern Turkey. *Geol. Soc. London Spec. Pub.*, **156**,
20
21 945 475-515.
22
23 946 Papanikolaou, D., Alexandri, M., Nomikou, P., Ballas, D., 2002. Morphotectonic structure of the
24
25 947 western part of the North Aegean Basin based on swath bathymetry. *Mar. Geol.*, **190**, 465-492.
26
27 948 Papanikolaou, D., Nomikou, P., Papanikolaou, I., Lampridou, D., Rousakis, G., Alexandri, M., 2019.
28
29 949 Active tectonics and seismic hazard in Skyros Basin, North Aegean Sea, Greece. *Mar. Geol.*, **407**, 94-
30
31 950 110.
32
33 951 Papatheodorou, G., Hasiotis, T., Ferentinos, G., 1993. Gas-charged sediments in the Aegean and Ionian
34
35 952 Seas, Greece. *Mar. Geol.*, **112**, 171–184.
36
37 953 Perouse, E., Chamot-Rooke, N., Rabaute, A., Briole, P., Jouanne, F., Georgiev, I., Dimitrov, D., 2012.
38
39 954 Bridging onshore and offshore present-day kinematics of central and eastern Mediterranean: im-
40
41 955 plications for crustal dynamics and mantle flow. *Geochem. Geophys. Geosyst.*, **13**,
42
43 956 <https://doi.org/10.1029/2012GC004289>.
44
45 957 Piper, D. J. & Perissoratis, C., 1991. Late Quaternary Sedimentation on the North Aegean Continental
46
47 958 Margin, Greece. *AAPG Bulletin*, **75**, 46–61.
48
49 959 Pe-Piper, G., Piper, D.J.W., Reynolds, P.H., 1983. Paleomagnetic stratigraphy and radiometric dating
50
51 960 of the Pliocene volcanic rocks of Aegina, Greece. *Bulletin volcanologique*, **46**, 1-7.
52
53 961 Porkoláb, K., Willingshofer, E., Sokoutis, D., Békési, E., Beekman, F., 2023. Post-5 Ma rock
54
55 962 deformation on Alonnisos (Greece) constrains the propagation of the North Anatolian Fault.
56
57 963 *Tectonophysics*, **846**, <https://doi.org/10.1016/j.tecto.2022.229654>
58
59
60

- 1
2
3 964 Proedrou, P. & Papaconstantinou, C.M., 2004. Prinos basin – a model for oil exploration. *Bulletin of the*
4
5 965 *Geological Society of Greece*, **36**, 327-333
6
7 966 Proedrou, P. & Sidiropoulos, T., 1992. Prinos field-Greece, Aegean basin, structural traps: treatise of
8
9 967 petroleum geology, atlas of oil and gas fields. *AAPG*, 275-291.
10
11 968 Rangin, C., Le Pichon, X., Demirbag, E., Imren, C., 2004. Strain localization in the Sea of Marmara:
12
13 969 Propagation of the North Anatolian Fault in a now inactive pull-apart. *Tectonics*, **23**,
14
15 970 doi.org/10.1029/2002TC001437
16
17 971 Rangin, C., 2005. The North Anatolian Fault: a new look. *Annual Review of Earth Planetary Sciences*,
18
19 972 **33**, 7-112, doi: 10.1146/annurev.earth.32.101802.120415
20
21 973 Rebesco, M., Hernández-Molina, F.J., Van Rooij, D., Wahlin, A., 2014. Contourites and associated
22
23 974 sediments controlled by deep-water circulation processes: state of the art and future considerations. *Mar.*
24
25 975 *Geol.*, **352**, 111-154.
26
27 976 Reicherter, K., Papanikolaou, I., Roger, J., Mathes-Schmidt, M., Papanikolaou, D., Rössler, S.,
28
29 977 Grützner, C., Stamatis, G., 2010. Holocene tsunamigenic sediments and tsunami modelling in
30
31 978 theThermaikos Gulf area (northern Greece). *Zeitschrift für Geomorphologie Supplementary issues*, **54**,
32
33 979 99–125.
34
35 980 Reilinger, R., et al., 2006. GPS constraints on continental deformation in the Africa–Arabia–Eurasia
36
37 981 continental collision zone and implications for the dynamics of plate interactions. *J. Geophys. Res.*, **111**,
38
39 982 B05411, doi:10.1029/2005JB004051.
40
41 983 Rodriguez, M., Sakellariou, D., Gorini, C., Chamot-Rooke, N., d’Acremont, E., Nercessian, A.,
42
43 984 Tsampouraki-Kraounaki, K., Oregioni, D., Delescluse, M., Janin, A., 2018. Seismic profiles across
44
45 985 the North Anatolian Fault in the Aegean Sea, in: *EGU General Assembly Conference Abstracts*
46
47 986 20: 7426.
48
49 987 Roussos, N. & Lyssimachou, T., 1991. Structure of the Central North Aegean Trough: an active strike-
50
51 988 slip deformation zone. *Basin Res.*, **3**, 39–48.
52
53 989 Rütter, E.H. & Valetti, L., 2019. Stretching transforms – Mediterranean examples from the Betic-
54
55 990 Alboran, Tyrrhenian-Calabrian and Aegean-Anatolia regions. *Transform plate boundaries and fracture*
56
57 991 *zones*, edited by: Duarte, J., chapter 12: 301-320.

- 1
2
3 992 Sakellariou, D. & Tsampouraki-Kraounaki, K., 2016. Offshore faulting in the Aegean Sea: A synthesis
4
5 993 based on bathymetric and seismic profiling data. *Bulletin of the Geological Society of Greece*, **50**, 124–
6
7 994 133.
- 8
9 995 Sakellariou, D. & Galanidou, N., 2017. Aegean Pleistocene landscapes above and below sea level:
10
11 996 palaeogeographic reconstruction and Hominin dispersals. Under the Sea: archeology and
12
13 997 palaeolandscapes of the continental shelf, Bailey G, Harff J, Sakellariou D eds (Springer), *Coastal*
14
15 998 *research library*, **20**, 335-359, doi 10.1007/978-3-319-53160-1
- 16
17 999 Sakellariou, D. & Tsampouraki-Kraounaki, K., 2018. Plio-Quaternary Extension and Strike-Slip
18
19 1000 Tectonics in the Aegean. *Transform Plate Boundaries and Fracture Zones*, edited by: Duarte, J., chap.
20
21 1001 14, 339-374.
- 22
23 1002 Sakellariou, D., Rousakis, G., Vougioukalakis, G., Ioakim, C., Panagiotopoulos, I., Morfis, I.,
24
25 1003 Zimianitis, E., Athanasoulis, K., Tsampouraki-Kraounaki, K., Mpardis, D., Karageorgis, A., 2016.
26
27 1004 Deformation pattern in the western North Aegean trough: pre-liminary results. *Bulletin of the Geological*
28
29 1005 *Society of Greece*, **50**, 134–143.
- 30
31 1006 Sakellariou, D., Rousakis, G., Morfis, I., Panagiotopoulos, I., Ioakim, C., Trikalinou, G.,
32
33 1007 Tsampouraki-Kraounaki, K., Kranis, H., Karageorgis, A., 2018. Deformation and kinematics at the
34
35 1008 termination of the North Anatolian Fault: the North Aegean Trough horsetail structure. *9th International*
36
37 1009 *INQUA Meeting on Paleoseismology, Active Tectonics and Archeoseismology (PATA), 25 – 27 June*
38
39 1010 *2018, Possidi, Greece, Proceedings*, 237-240.
- 40
41 1011 Schettino, A. & Turco, E., 2011. Tectonic history of the western Tethys since the Late Triassic. *GSA*
42
43 1012 *bulletin*, **123**, 89-105.
- 44
45 1013 Sengör, A.M.C., Tüysüz, O., Imren, C., Sakinc, M., Eyidogan, H., Görür, N., LePichon, X.,
46
47 1014 Sengör, A.M.C., Grall, C., Imren, C., LePichon, X., Görür, N., Henry, P., Karabulut, H., Siyako, M.,
48
49 1015 2014. The geometry of the North Anatolian transform fault in the Sea of Marmara and its temporal
50
51 1016 evolution: implications for the development of intracontinental transform faults. *Canadian Journal of*
52
53 1017 *Earth Sciences*, **51**, 222-242, dx.doi.org/10.1139/cjes-2013-0160
- 54
55
56
57
58
59
60

- 1
2
3 1018 Sengör, A.M.C., Zabcı, C., Nata'in, B.A., 2019. Continental transform faults: congruence and
4
5 1019 incongruence with normal plate kinematics. *Transform Plate Boundaries and Fracture Zones*, Edited
6
7 1020 by Joao Duarte, Elsevier 170-246
8
9 1021 Siyako, M. & Huvaz, O., 2007. Eocene stratigraphic evolution of the Thrace Basin. *Turk. Sediment.*
10
11 1022 *Geol.*, **198**, 75-91.
12
13 1023 Shillington, D.J., Seeber, L., Sorlien, C.C., Steckler, M.S., Kurt, H., Dondurur, D., Çifçi, G., İmren, C.,
14
15 1024 Cormier, M.H., McHugh, C.M.G., Gürçay, S., Poyraz, D., Okay, S., Atgın, O., Diebold, J.B., 2012.
16
17 1025 Evidence of widespread creep on the flanks of the Sea of Marmara transform basin from marine
18
19 1026 geophysical data. *Geology*, **40**, 439–442
20
21
22 1027 Sodoudi, F., Kind, R., Hatzfeld, D., Priestley, K., Hanka, W., Wylegalla, K., Stavrakakis, G., Vafidis,
23
24 1028 A., Harjes, H.-P., Bohnhoff, M., 2006. Lithospheric structure of the Aegean obtained from P and S
25
26 1029 receiver functions. *J. Geophys. Res. Solid Earth*, **111**, <https://doi.org/10.1029/2005JB003932>
27
28 1030 Sprovieri, M., Ribera d'Alcalà, M., Manta, D.S., Bellanca, A., Neri, R., Lirer, F., Taberner, C., Pueyo,
29
30 1031 J.J., Sammartino, S., 2008. Ba/Ca evolution in water masses of the Mediterranean late Neogene.
31
32 1032 *Paleoceanography*, **23**(PA3205), doi:10.1029/2007PA001469
33
34 1033 Suc, J.-P., Popescu, S.-M., Do Couto, D., Clauzon, G., Rubino, J.-L., Melinte-Dobrinescu, M., C.,
35
36 1034 Quillévéré, F., Brun, J.-P., Du-murdžanov, N., Zagorchev, I., Lesiæ, V., Tomiæ, D., Meyer, B., Macalet,
37
38 1035 R., Rifelj, H., 2015. Marine gateway vs. fluvial stream within the Balkans from 6 to 5 Ma. *Mar. Pet.*
39
40 1036 *Geol.*, **66**, 231–245.
41
42
43 1037 Sümer, Ö., Uzel, B., Özkaymak, C., Sözbilir, H., 2018. Kinematics of the Havran-Balikesir Fault Zone
44
45 1038 and its implication on geodynamic evolution of the Southern Marmara Region, NW Anatolia.
46
47 1039 *Geodinamica acta*, **30**, 306-323, <https://doi.org/10.1080/09853111.2018.1540145>
48
49 1040 Tchalenko, J.S., 1970. Similarities between shear zones of different magnitudes. *Geol. Soc. America*
50
51 1041 *Bull.*, **81**, 1625-1640.
52
53 1042 Tchalenko, J.S. & Ambraseys, N.N., 1970. Structural Analysis of the Dasht-e Bayaz (Iran) Earthquake
54
55 1043 Fractures. *Geological Society of America Bulletin*, **81**, 41-60.
56
57 1044 Tsampouraki -Kraounaki, K., Sakellariou, D., Rousakis, G., Morfis, I., Panagiotopoulos, I., Livanos, I.,
58
59 1045 Manta, K., Paraschos, F., Papatheodorou, G., 2021. The Santorini-Amorgos Shear Zone: evidence for

- 1
2
3 1046 dextral transtension in the South Aegean back-arc region, Greece. *Geosciences*, **11**, doi:
4
5 1047 10.3390/geosciences11050216
6
7 1048 Tripsanas, E.K., Panagiotopoulos, I.P., Lykousis, V., Morfis, I., Karageorgis, A.P., Anastasakis, G.,
8
9 1049 Kontogonis, G., 2016. Late quaternary bottom-current activity in the south Aegean Sea reflecting
10
11 1050 climate-driven dense-water production. *Mar. Geol.*, **375**, 99-119.
12
13 1051 Turgut, S., Eseller, G., 2000. Sequence stratigraphy, tectonics and depositional history in eastern Thrace
14
15 1052 Basin, NW Turkey. *Mar. Pet. Geol.*, **17**, 61-100.
16
17 1053 Varesis, A. & Anastasakis, G., 2021. Cenozoic marine basin evolution in the western North Aegean
18
19 1054 Trough margin: seismic stratigraphic evidence. *Water*, **13**, 2267. <https://doi.org/10.3390/w13162267>
20
21 1055 Vigny, C., Socquet, A., Rangin, C., Chamot-Rooke, N., Pubellier, M., Bouin, M.-N., Bertrand, G.,
22
23 1056 Becker, M., 2003. Present-day crustal deformation around Sagaing fault, Myanmar. *J. Geophys. Res.*,
24
25 1057 **108**, 2533. <http://dx.doi.org/10.1029/2002JB001999>
26
27 1058 Wesnousky, S.G., 2005. The San Andreas and Walker Lane fault systems, western North America:
28
29 1059 transpression, transtension, cumulative slip and the structural evolution of a major transform plate
30
31 1060 boundary. *J. Struct. Geol.*, **27**, 1505-1512.
32
33 1061 Woodcock, N. H., Daly, M.C., 1986. The role of strike-slip fault systems at plate boundaries. *Phil.*
34
35 1062 *Trans. R. Soc. A*, **317**, 13-29.
36
37 1063 Yalçın, H., Kürçer, A., Utkucu, M., Gülen, L., 2016. Seismotectonics of the southern marmara region,
38
39 1064 NW turkey. *Bulletin of the Geological Society of Greece*, **50**, 173-181.
40
41 1065 <http://dx.doi.org/10.12681/bgsg.11717>.
42
43
44
45 1066
46
47
48
49
50
51
52
53
54
55
56
57
58
59
60